JOURNAL OF PETROLOGY | VOLUME 0 | NUMBER 0 | PAGES 1–27 | 2011 | doi:10.1093/petrology/egr040
Journal of Petrology Advance Access published August 25, 2011

Hydrous, Low-carbon Melting of Garnet Peridotite

J. BRIAN BALTA*, PAUL D. ASIMOW AND JED L. MOSENFELDER

DEPARTMENT OF GEOLOGICAL AND PLANETARY SCIENCES, CALIFORNIA INSTITUTE OF TECHNOLOGY, PASADENA, CA 91125, USA

RECEIVED JUNE 25, 2010; ACCEPTED JULY 26, 2011

The presence of volatile species in the Earth's upper mantle drives the formation of low-degree melts at pressures and temperatures at which volatile-free mantle rocks would be subsolidus. The two most abundant volatile species, given the oxidation state of the Earth's upper mantle, are carbon dioxide and water; each species has a distinct effect on the melting process. We present experimental melting results from 3 GPa and 1375°C on hydrous systems with controlled water contents and rigorously minimized carbon contamination that constrain the independent effects of these volatiles. The hydrous melts in these experiments are in equilibrium with garnet peridotite at pressures reasonable for hydrous melting under mid-ocean ridges. Compared with anhydrous experiments or carbon-rich silicate melting, the addition of water produces a melt with increased SiO_2 content relative to MgO and FeO, tantamount to an increase in the stability of olivine at the solidus relative to the other crystalline phases. We also report a substantial and unexpected change in the composition of clinopyroxene in equilibrium with the melt; the clinopyroxene stability field contracts when water is added to the system, producing clinopyroxenes with higher CaO and lower Al_2O_3 than found at the same pressure without water. The contraction of the clinopyroxene field decreases the bulk partition coefficients of TiO_2, Na_2O, heavy rare earth elements, U, and H_2O, with important implications for hydrous melting of the mantle; for example, initiating hydrous melting deeper in the garnet lherzolite stability field.

KEY WORDS: *mantle; peridotite melting; volatiles; water*

INTRODUCTION

Water plays a fundamental role in the melting of the Earth's mantle. It interacts strongly with other components in non-ideal silicate melt solutions and therefore has direct effects on melt chemistry. Furthermore, the presence of a volatile species in upwelling mantle will allow a source rock to melt at higher pressures and lower temperatures than it would if it were volatile-free, implying an indirect but significant effect on liquid composition owing to melting in the presence of different mineral assemblages. Understanding the effects of water on the melting of the Earth's mantle therefore requires experiments on natural compositions (or close analogues) across the substantial range of temperatures, pressures, and compositions relevant to modern melting regimes.

Pioneering early work on hydrous melting of mantle-like compositions was conducted by Kushiro and co-workers, on simplified systems such as enstatite–H_2O (Kushiro, 1968), forsterite–enstatite–diopside–H_2O (Kushiro, 1969), and forsterite–diopsite–silica–H_2O (Kushiro, 1972). One important result of these experiments is that the presence of dissolved water in a silicate melt in equilibrium with solids tends to drive the melt to higher silica contents. This change is explained by the reaction between water and bridging oxygens in the tetrahedral silicate network, which depolymerizes the liquid and lowers the activity coefficient of silica (Mysen *et al.*, 1980).

A full accounting for the effect of water on the melting column must involve hydrous experiments on more complex systems, including those without a free vapor phase where the activity of water is not fixed (as commonly occurs in the mantle away from subduction zone inputs). Gaetani & Grove (1998) conducted experiments on hydrous basaltic liquids in equilibrium with synthetic lherzolite and harzburgite lithologies at pressures from 1·2 to 2 GPa. Falloon & Danyushevsky (2000) and Parman & Grove (2004) produced hydrous melts in equilibrium with

*Corresponding author. Present address: Department of Earth and Planetary Sciences, University of Tennessee, Knoxville, TN 37909, USA. Telephone: 865-974-3874. Fax: 865-974-2368. E-mail: jbalta@utk.edu

harzburgite lithologies from 1·5 to 2·5 GPa and 1·5 to 2·2 GPa, respectively. Liu *et al.* (2006) reported experiments on hydrous melts in equilibrium with a simplified spinel lherzolite at 1·2 GPa pressure. Wood & Turner (2009) compiled these studies and estimated the relationships between water content and melt compositional variables such as wt % MgO and SiO_2.

Although the above studies provide valuable information about the effect of water on melting, there are important differences between them and the style of hydrous melting likely to occur under mid-ocean ridges. First, under a mid-ocean ridge, water will flux a low-degree melt at greater depths than those sampled by the experiments if the peridotite contains a few hundred ppm water by weight (Asimow & Langmuir, 2003). If hydrous melting occurs in the garnet lherzolite field (Asimow *et al.*, 2004), the solid mineralogy and the partitioning of elements will be significantly different from those at lower pressures. Second, experiments conducted on analogue systems or in equilibrium with harzburgitic lithologies may also show compositions and partitioning significantly different from those in equilibrium with lherzolite. As hydrous melting is likely to produce only low-degree melts, it is unlikely that their production would deplete the solid residue enough to produce a harzburgite; higher degrees of melting at lower pressures would be required (e.g. Kelemen *et al.*, 1992; Asimow *et al.*, 1999). Finally, as noted by Liu *et al.* (2006) and Wood & Turner (2009), a common concern with hydrous melting experiments at any condition has been infiltration of carbon into the experimental charges. As carbon and water have a strong mutual interaction in silicate melts, the presence of variable amounts of carbon in a hydrous melt will affect the activity of water and other reactive species.

Whether melt is produced in the garnet lherzolite stability field under mid-ocean ridges in particular has been a longstanding issue. The trace element and isotopic characteristics of mid-ocean ridge basalts (MORB) have been interpreted to suggest that garnet is a necessary residual phase in the melting zone (e.g. Salters & Hart, 1989; Shen & Forsyth, 1995). However, this constraint is apparently at odds with the high potential temperatures required to encounter the peridotite solidus in the garnet field and the high crustal thicknesses predicted for such hot melting regimes (Iwamori *et al.*, 1995; Robinson & Wood, 1998). A number of solutions have been proposed to resolve this controversy, such as melting of distinct pyroxenite lithologies in the MORB source (Hirschmann & Stolper, 1996), cessation of melting well below the base of the crust (Shen & Forsyth, 1995), or increased compatibility of rare earth elements (REE) in aluminous clinopyroxene (cpx) at high pressures (Blundy *et al.*, 1998). Each of these explanations for the garnet signature has potential complications. The experiments of Pertermann & Hirschmann (2003*b*) show that pyroxenite cannot make up more than 2% of the MORB source region. The Shen & Forsyth (1995) model is inconsistent with thermodynamic expectations (e.g. Asimow *et al.*, 1999), implies a correlation between crustal thickness and spreading rate that is not observed (White *et al.*, 1992), and is inconsistent with the abundances of Na_2O and SiO_2 in MORB (Kinzler, 1997). The partition coefficients (D = concentration of species in solid/concentration of species in liquid) of Blundy *et al.* (1998) differ from those of other researchers (e.g. Salters & Longhi, 1999) and require highly aluminous cpx that may not exist in certain circumstances, as we discuss below. Thus, the origin of the garnet signature in MORB remains an open question.

We have designed and conducted experiments with these issues in mind to illustrate the effects of limited quantities of water on the melting of garnet-rich fertile peridotite under low-carbon conditions. These experiments show, first, that the effect of water on the overall liquid composition is similar to that found by Gaetani & Grove (1998) on carbon-bearing, lower pressure samples: the presence of water decreases the ratio of $(MgO + FeO)/SiO_2$ and thus increases the SiO_2 content of the liquid if considered on a volatile-free basis. Second, we show that carbon, even at low concentrations, interacts with water in the liquid and may counteract the effect of water on melt chemistry. Third, we show that the interaction of hydrous melts with a fertile peridotite mineralogy has significant and unexpected effects on the modal abundance and composition of cpx during melting, with implications for partitioning of cpx-hosted elements. An additional observation of the compatibility of MnO in garnet and its consequences has been explored by Balta *et al.* (2011*a*).

METHODS

Experimental approach

Producing equilibrium, low-degree melts has historically been a difficult problem in experimental petrology, as it is much easier to sample and analyze high-degree melts. Two approaches have been explored: extraction methods and 'sandwich' methods. The first method is based on the maintenance of open pore space or highly wetting surfaces towards which low-degree melts can segregate during experiments. Johnson & Kushiro (1992), Kushiro & Hirose (1992), Hirose & Kushiro (1993), Baker & Stolper (1994), Baker *et al.* (1995) and Van den Bleeken *et al.* (2011) employed a diamond-aggregate technique, where the pore space between diamond crystals was used to trap the extracted initial melts. The rapidly extracted melt is intended to equilibrate with interstitial melt in the solid pile and then to quench to an unmodified glass because nucleation sites are absent. Modifications of this technique include crimped capsule or foil layers (Holloway & Kawamoto, 1997), vitreous carbon spheres (Schwab & Johnston, 2001;

Wasylenki *et al.*, 2003; Pertermann & Hirschmann, 2003*a*), and microdikes of melt formed during graphite capsule compression (Laporte *et al.*, 2004). For our experiments, the diamond-aggregate technique would be inappropriate, as the presence of diamond or vitreous carbon would provide an immediate source of carbon and vitreous carbon spheres are known to take up water (Wasylenki *et al.*, 2003). The presence of carbon-rich phases would also make accurate determinations of dissolved carbon contents difficult (Pertermann & Hirschmann, 2003*a*).

'Sandwich' experiments attempt to produce analyzable pools of melt large enough to escape quench modification by reacting a melt of a composition close to the predicted low-degree melt with solids until the liquid becomes multiply saturated with the solids (Stolper, 1980; Takahashi & Kushiro, 1983). Several improvements to this method have been proposed. One difficulty is that the solid compositions tend to change as they react with the liquids, producing solids and liquids that are in equilibrium with each other, but that are not necessarily representative of the mantle. Wallace & Green (1988) and Robinson *et al.* (1998) used an iterative procedure, where each successive liquid begins at the composition measured in the previous experiment and reacts with a new batch of the original solid until the liquid and solid compositions no longer evolve during the run. This improves on the multiple-saturation technique by making the solid compositions more representative of the mantle. However, because our ability to measure compositions is limited by the analytical error of the electron microprobe, it is possible for liquids with a range of compositions to exist at equilibrium with solids that are indistinguishable within error from the starting material. Moreover, in the case of highly compatible or highly incompatible elements, it is possible that the liquid and solid compositions can be trapped in metastable local minima or that many iterations will be required to approach equilibrium.

Hirschmann & Dasgupta (2007) proposed a new approach that they called 'modified iterative sandwich experiments' (MISE): the solid/melt partition coefficients measured in each iteration are used to calculate the next liquid using the batch melting equation evaluated in the limit of zero melt fraction. However, producing a final equilibrated liquid remains challenging, particularly for hydrous systems. First, very low or very high partition coefficients cannot be accurately measured owing to low concentration in one phase, a particularly important issue for water. Water is hosted in multiple phases, has partition coefficients that change as a function of mineral composition, and has large possible ranges in the total solid water content (e.g. Hirschmann *et al.*, 2009). Second, convergence requires that the minerals of the starting assemblage do not evolve during the final experiment, whereas, as we show below, the introduction of hydrous melts in our experiments consistently causes a shift in cpx composition that makes it unclear how to obtain the proper modal abundance of the solid phases and hence the proper bulk partition coefficients by mass balance. Finally, this technique does not guarantee that the oxides will sum to 100% after its application, and therefore requires a choice to either exclude a closure component from the calculation or to renormalize the calculated near-solidus liquid composition, neither of which is an optimal solution.

For our experiments, we attempted to replicate the MISE procedure of Hirschmann & Dasgupta (2007), but because of unique experimental challenges in the water + garnet peridotite system, which we discuss in the next sections, we could not achieve a single MISE-equilibrated liquid. Instead, we obtained a family of multiply saturated liquid compositions after a multi-step procedure. First we carried out two iterations using a hybrid of the iterative sandwich and MISE techniques. We reacted a hydrous candidate liquid with solid garnet peridotite, measured the mineral/melt partition coefficients and then applied the MISE technique to calculate the concentrations of most of the oxides in the next candidate liquid. For very incompatible elements such as K_2O, very compatible elements such as MgO, and for elements such as SiO_2 where the MISE forecasting method is unstable or compromised by a large correction for closure, we simply adopted the measured concentration in the melt for the next candidate liquid. This hybrid approach may overcome some pitfalls in the MISE method, by reducing the degree of the closure correction and eliminating large corrections for certain elements.

After iterations, we obtained hydrous basalt composition multiply saturated with olivine, clinopyroxene, and garnet. However, these runs also established that issues of capsule preparation, welding, diffusion, and even inner capsule position within the outer capsule preclude control of water content to a degree accurate enough to obtain convergence of the iterations for the water component. Therefore, instead of attempting to produce a single liquid representative of mantle melting at known water content, we exploited the uncertainty in final water content by repeating the third iteration several times, obtaining a range of equilibrium assemblages of garnet, olivine, clinopyroxene, and hydrous liquid with variable water contents. This choice allowed us to examine the behavior of peridotite melting across a range of water contents and to constrain the relationship between the contents of water, carbon, alkalis and silica in the liquid.

Solid preparation

A major concern for our experiments was the initial state of the solids added during each run. The equilibrium we want to observe is between hydrous liquid and fertile garnet peridotite. Most of the commonly available natural

Table 1: Measured compositions of solid phases from subsolidus recrystallized peridotites

	KLB-1 + Al_2O_3	NX-08[1]	CPX[2]	Olivine	Garnet	Az Gt[3]	R377 OPX[4]
SiO_2	43·33	45·42	53·54(73)	40·91(76)	42·64(44)	41·83(68)	55·60(28)
TiO_2	0·11	0·64	0·26(1·6)	0·007(0·6)	0·23(1·5)	0·076(1·8)	0·063(0·6)
Al_2O_3	6·28	12·39	6·85(35)	0·13(14)	22·29(28)	23·30(35)	5·642(27)
FeO	8·27	10·82	4·19(19)	9·87(61)	6·66(11)	8·86(37)	6·06(23)
MnO	0·12	0·1	0·10(1·4)	0·10(1·7)	0·19(1·7)	0·32(2·5)	0·10(1·9)
MgO	38·08	16·18	19·79(88)	49·07(83)	22·46(25)	20·67(66)	31·30(21)
CaO	2·98	9·33	12·82(53)	0·18(6·8)	4·75(13)	4·22(9·2)	1·90(9·1)
Na_2O	0·29	2·76	1·98(9·1)	0·03(1·1)	0·03(2·2)	0·03(1·1)	0·33(3·4)
K_2O	b.d.	0·22	b.d.(0·5)	b.d.(0·4)	b.d.(0·7)	b.d.(0·6)	b.d.(0·3)
NiO	0·24	0·01	0·07(2·4)	0·32(8·6)	b.d.(1·6)	b.d.(2·3)	b.d.(1·7)
Cr_2O_3	0·31	0·13	0·54(3·2)	0·05(1·9)	0·87(4·6)	0·30(2·5)	0·45(5·4)
Totals	100	98	100·20(71)	100·74(64)	100·21(66)	99·66(128)	101·51(26)
Mg-no.			0·893	0·898	0·857	0·805	0·901
Modal abundance[5]			0·14	0·62	0·24		

Values in parentheses are 100 × the standard deviation of the electron microprobe analyses. b.d., below detection limit.
[1]Starting basalt composition for reported experiments; 2% H_2O added as $Al(OH)_3$.
[2]Analyses on >30 grains of each mineral, with only 1–2 analyses per grain.
[3]Composition of the garnet seed that was added to the peridotite mixture.
[4]Comes from an earlier step in the iteration.
[5]Modal abundances calculated by mass balance considering possible addition of Al_2O_3. χ^2 value for fit is 2.04.

fertile peridotites, however, are spinel or plagioclase peridotites owing to reaction at low pressures.

To produce our experimental solid peridotite, we began with a sample of natural KLB-1 peridotite powder of variable grain size (kindly supplied by C. Herzberg, from the same powder as the original KLB-1 of E. Takahashi). Grain mount analysis showed a mix of grain sizes up to nearly 100 μm, much too large to re-equilibrate on the timescales of the experiments. Given our focus on obtaining melts in equilibrium with garnet peridotite, we chose to aggressively grind the mixture to reduce the grain size sufficiently to fully recrystallize the starting material. The KLB-1 powder was mixed with <1% by weight magnesian garnet from Garnet Ridge, Arizona (supplied by G. R. Rossman; composition given in Table 1) to give seed grains for garnet growth during sub-solidus reaction. This mixture was ground for several hours in an alumina mortar and pestle to reduce the maximum grain size from ~100 μm to ~1 μm, allowing for sub-solidus recrystallization on reasonable timescales. Unfortunately, this grinding step introduced alumina contamination to the starting material, increasing the Al_2O_3 of the starting material by ~3 wt %.

For each experiment, the powder was dried and packed into a compound molybdenum–gold–palladium–iron capsule. The capsule was prepared by submersing an ~10 mm long, 3 mm outer diameter (o.d.) $Au_{75}Pd_{25}$ capsule in Kilauea 1919 basalt at 1190°C for 48 h under a controlled H_2–CO_2 gas stream at fO_2 1·6 log units below the quartz–fayalite–magnetite (QFM) buffer, following the technique outlined by Balta *et al.* (2011*b*). This produced a capsule with ~4% dissolved Fe. The presence of Fe tended to make the capsule brittle and likely to tear when compressed, so this capsule was hammered into a molybdenum sheath to prevent tearing. The sheath was made by drilling a 3 mm diameter well into a 4 mm o.d. molybdenum rod, maintaining one closed end. A 1 mm thick lid cut from the same stock covered the other end during the high-pressure experiment. The filled, compound capsule was heated to 1000°C under an H_2–CO_2 gas stream with fO_2 set 2·0 log units below the QFM buffer, within the range of predicted mantle values (Frost & McCammon, 2008). This step devolatilized the peridotite without oxidizing it. The capsule was kept at 300°C until the gold–palladium was welded shut. The molybdenum lid was placed on top of the capsule and cold-welded to the remainder of the capsule upon compression.

All of our experiments were conducted at a nominal pressure of 3 GPa in an end-loaded piston-cylinder device. We used ½ inch pressure cells composed of an outer sheath of calcium fluoride, a straight-walled graphite heating element, and crushable MgO spacers to center the capsule in the hot spot. Temperature was monitored during the run using a $W_{95}Re_5$–$W_{74}Re_{26}$ thermocouple (type C),

with no pressure correction on the e.m.f., and typical temperature fluctuations of 2°C or less. Experiments were first placed at pressure and allowed to compact for at least an hour before heating; this technique seems to help improve the capsule seal. Pressure calibration experiments based on the 1300°C, 2·85 GPa reaction of 3 anorthite = grossular + 2 kyanite + quartz, determined by Koziol & Newton (1988), located the reaction between nominal pressures of 2·83 and 2·93 GPa, suggesting that pressure correction is negligible to better than 0·1 GPa (Supplementary Data Table 1, available for downloading at http://www.petrology.oxfordjournals.org). The recrystallization runs were held below the solidus of KLB-1 (Herzberg, 2000) at 1350°C and 3 GPa for a period of at least 336 h. The run times were long enough to homogenize the sample to the level measurable by electron microprobe in all analyzed major and trace elements except for NiO, which declines near the capsule wall owing to Ni loss to the capsule. Temperature gradients within the capsule have not been calibrated, but the homogeneity of the final samples suggests that they are limited to <20°C in both the sub-solidus and the melting experiments.

Liquid preparation

The hydrous liquid in our experiments was synthesized from laboratory grade oxides, carbonates, and hydroxides. The initial seed liquid for the iteration was the calculated near-solidus liquid with 1 wt % H_2O in equilibrium with KLB-1 peridotite at 3 GPa according to the pHMELTS algorithm (Smith & Asimow, 2005), with further liquids synthesized based on the resulting liquid compositions. The mix was initially made with an Al_2O_3 deficit, as H_2O would be later added as gibbsite [$Al(OH)_3$]. Oxide and carbonate reagents were first dried separately, mixed by weight, ground under ethanol for >8 h, and step-heated at 100°C h^{-1} to 800°C in air to decarbonate the mixture. The mixture was then placed at 1000°C for ~12 h at $fO_2 = 10^{-13}$ bars to convert most of the iron to Fe^{2+}. It was then heated in a platinum crucible to 1460°C in an H_2–CO_2 gas stream with an fO_2 2·0 log units below the QFM buffer, for 1 h. The crucible was iron-preconditioned using the technique of Kessel *et al.* (2001) to avoid iron loss. Na_2O is expected to be the most volatile element during this procedure (e.g. Tsuchiyama *et al.*, 1981); no significant Na_2O loss was observed during sample preparation. The liquid was quenched to a glass by immersing the crucible in water. The glass was then broken apart and re-ground for 4 h along with powdered gibbsite as a water source, with the amount calculated to make up for the missing Al_2O_3 and to provide several wt % H_2O. Gibbsite was used because we were able to verify, using a high-temperature pyrolysis elemental-analyzer connected to an isotope-ratio mass spectrometer, that the gibbsite was carbon-free; other water-containing minerals, such as brucite, have been found to be carbon-contaminated and cannot be used for controlled-carbon experiments (e.g. Kelly *et al.* 1998; Sessions, 2006). Previous workers (e.g. Sisson *et al.* 2005; Alonso-Perez *et al.*, 2009) have suggested that grinding under ethanol could contaminate samples with carbon; however, with the elemental-analyzer we verified to better than 10 ppm that no carbon residue remained on the powder after drying.

Capsule design for melting experiments

Our capsule design was critical to maintaining hydrous conditions while avoiding carbon infiltration or other changes in parameters such as fO_2 that could affect the equilibrium liquid composition. We adapted the double-capsule design of Kägi *et al.* (2005), which was originally used to minimize variation in fO_2 and volatiles in hydrous experiments. An inner capsule of iron-preconditioned $Au_{75}Pd_{25}$, 1·6 mm o.d. and ~5 mm long, was loaded with roughly equal proportions of the recrystallized garnet peridotite and powdered hydrous glass. After welding (see below), this inner capsule was loaded along with more of the same powdered hydrous glass and extra liquid water (inserted by micro-syringe) into an outer capsule of iron-preconditioned Pt, 3·8 mm o.d. and ~10 mm long prior to compaction (Fig. 1). The extra water was loaded because diffusion of hydrogen through platinum is faster than through $Au_{75}Pd_{25}$ (e.g. Chou, 1986). Both the outer and inner capsule were arc welded with the cold end immersed in a bath of liquid N_2 to limit dehydration during welding, a major issue for the smaller capsules. The inner capsule was Fe-preconditioned using the calibration of Balta *et al.* (2011*b*), and the outer capsule was Fe-preconditioned using the calibration of Kessel *et al.* (2001). The outer capsule contained up to 20 times more glass than the inner capsule and served as a large reservoir to slow diffusion of carbon into the capsule from the graphite heating element in the cell.

Melting experiments

Melting experiments were run in the piston-cylinder using the same protocol as described above for the subsolidus recrystallization experiments except for temperature and time. Melting was conducted at 1375°C for periods from 6 to 20 h. No correlation was found between any measured property (including volatile content) and time. Temperature was chosen to be well below the solidus of volatile-free peridotite and low enough to avoid melting of the $Au_{75}Pd_{25}$ capsule (which was observed at over 1400°C) but still high enough to approach equilibrium between the solid and liquid in the charges. Quenching hydrous basaltic glasses from high pressures is challenging. Our experiments were quenched by shutting off the power and simultaneously releasing the oil pressure in the master ram cylinder; this achieved quench from the run temperature to <200°C in less than 10 s. This technique

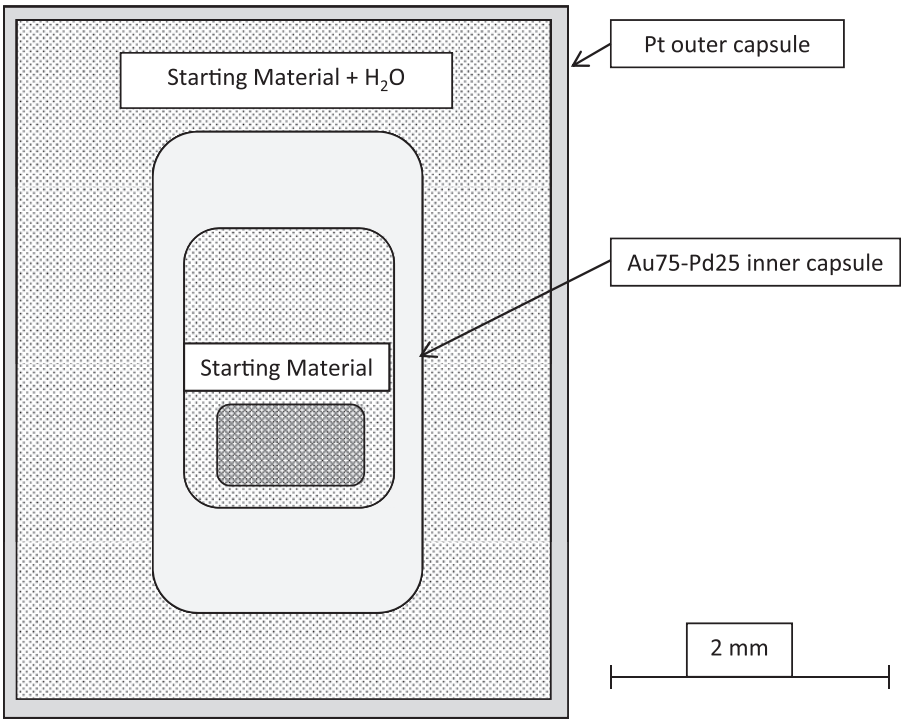

Fig. 1. Schematic capsule design. Lighter gray material in the inner capsule is loaded synthetic glass, the darker material is loaded peridotite. Peridotite was loaded in traditional sandwich format, with upper and lower layers, but the upper layer always sank to the bottom of the inner capsule. Melt percolation throughout the peridotite layer was complete. No vertical or horizontal exaggeration.

was similar to that employed by Putirka *et al.* (1996); however, we did not drop the pressure as aggressively prior to quenching because too fast a pressure drop could have caused decompression melting of the capsules. This technique allowed recovery of large volumes of crystal-free glass and obvious vesiculation on quench was not observed.

Analytical techniques

Major elements

Capsules were sectioned using a wire saw. One half of the capsule was mounted in and vacuum-impregnated with epoxy, polished using alumina and diamond grits, and carbon coated for analysis by electron microprobe and scanning electron microscope. Quantitative analyses were conducted using the JEOL JXA-8200 electron microprobe at the California Institute of Technology in wavelength-dispersive mode. Liquid compositions were measured using a current of 10 nA and a spot size of 15–20 μm, with 20 s counted on-peak and 10 s counted off-peak. Na and K were counted first to minimize loss of volatile elements. Lower current analyses were also performed to confirm that Na and K were not being lost. Solid phases were analyzed using a focused beam, a current of 30–40 nA, and identical counting times.

Volatile species

Volatile contents in the glasses were measured by Fourier transform infrared spectrometry (FTIR) using a Nicolet Magna 860 system coupled to a Spectra-Tech Continuum microscope. Spectra were obtained on doubly polished sections of the experiments from 1000 to 6000 cm^{-1} using unpolarized light, a KBr beamsplitter, and an MCT-A detector. Sample thickness and flatness were checked using a digital micrometer close to the analyzed spots; wedging was limited to a few micrometers. We used rectangular apertures greater than 30 μm in the short direction and attempted to avoid contamination by solid phases, cracks, and edges. Multiple spots were measured to establish homogeneity of volatile contents (better than 10% across single runs). Water contents were calculated from absorbances of bands near 5200 and 4500 cm^{-1} based on the composition-dependent calibration of Ohlhorst *et al.* (2001) and electron probe analyses of the major-element glass composition. Extrapolation was required, as the lowest SiO_2 content used in the calibration was 50 wt % whereas our liquids have ~45 wt % SiO_2. CO_3 contents were calculated using the calibration of Fine & Stolper (1986) of the peak near 1435 cm^{-1}. Molecular CO_2 contents were calculated using the calibration of Morizet *et al.* (2002) for the peak near 2340 cm^{-1}.

Glass densities were calculated using the iterative technique of Aubaud *et al.* (2007), although their calibration does not include carbonate. Linear background corrections were used, potentially giving small additional errors on each analysis.

We estimate the relative error on the volatile content measurements to be ~10% (1σ) based on the repeat analyses of single samples, which is sufficient for the purposes of this study. The largest sources of error are measurement of the sample thickness at the site of analysis and uncertainty in the absorption coefficient. Typically the absolute error is less than ±0·5 wt % H_2O. Reduced errors on similar analyses are probably possible in the future, but would require a more detailed understanding of the relationship between the multiple peaks near 4500 cm^{-1} (see below) and the total water content, as well as calibration of absorption coefficients across a wider range of silicate liquid compositions including picritic basalts with variable amounts of carbonate (see below).

To confirm the applicability of our chosen calibration, we analyzed several samples at different thicknesses, allowing us to calculate water contents based on the OH^- stretching band at ~3600 cm^{-1} for comparison with the combination stretching and bending modes at ~5200 and ~4500 cm^{-1}. For the 3600 cm^{-1} peak, we used the calibration of Dixon *et al.* (1995) for basaltic liquids for which the absorption coefficient is precisely known and not strongly dependent on composition (Dixon *et al.*, 1997). For the combination bands, sample thicknesses of >100 μm were commonly used, whereas sample thicknesses <50 μm were necessary to bring the 3600 cm^{-1} peak on scale. These repeat measurements at different thicknesses and typically on different spots produced total water contents on single samples that were within 2% of each other, significantly less than the estimated analytical error.

MELTS calculations

For comparison with our experimental liquid composition, we calculated hydrous, low-degree silicate melt compositions using pHMELTS (Smith & Asimow, 2005). We used the solid KLB-1 composition, edited to improve the calculation by avoiding elements that the algorithm does not treat well. Specifically, we excluded K_2O, which MELTS treats as perfectly incompatible in mantle assemblages (causing a high-K low-degree melt to exist at all temperatures), and Mn, which is missing from the MELTS models of all mantle solids except olivine and which was not included in the pMELTS liquid calibration (Ghiorso *et al.*, 2002). The calculations were performed in two ways to ensure that the algorithm was not being caught in local minima. First, we calculated the equilibrium melt composition at 3 GPa and 1375°C, beginning with excess water. We decreased the available water content until the melt composition did not change significantly at each step. Second, we started the calculation subsolidus and found the initial melt composition during heating, varying the water content until the solidus was reached at 1375°C. This dual approach constitutes a sort of numerical reversal experiment and produces similar calculated compositions.

RESULTS

Recrystallization experiments

We produced several nearly identical sub-solidus peridotites from our KLB-1 starting mix showing no obvious evidence for zonation (Fig. 2) other than in NiO, which we interpret as evidence for close approach to equilibrium (Parman & Grove, 2004). The texture showed additional evidence of equilibrium, with subhedral to euhedral grain shapes and well-developed triple grain junctions. The peridotites consisted of mixtures of olivine, cpx, and garnet. No orthopyroxene (opx) was observed in any experiment, probably owing to the addition of Al_2O_3 in the process of grinding. Final grain sizes were between 5 and 20 μm for all phases. Average mineral compositions are reported in Table 1. Olivine Mg-numbers [=100 × molar MgO/(MgO + FeO)] averaged 89·8, consistent with fertile upper mantle and suggesting limited iron loss to the capsule. Using the bulk KLB-1 composition given by Davis *et al.* (2009) and our measured mineral compositions, we estimated modal abundances by least-squares mass balance, treating bulk Al_2O_3 content as a free parameter. Mineral compositions and calculated modal abundances are given in Table 1.

Hydrous melting experiments

All reported experiments produced hydrous, low-carbon basaltic glass in equilibrium with solid garnet, cpx, and olivine (Fig. 3). Opx was observed only in an initial experimental step that started with a higher silica liquid; none was observed in equilibrium with the final estimated solidus liquid composition, consistent with the lack of opx in the garnet peridotite starting material. A single opx composition from an early iteration is reported in Table 1 for comparison with opx measured by others in anhydrous experiments. The double-capsule technique was successful at limiting carbon diffusion when the inner capsule remained intact. In several experiments we were unable to measure cpx compositions because of quench overgrowths on small grains. However, in these experiments, the outer capsule crystallized measurable amounts of the equilibrium solid phases on its own, giving two separate liquid–solid pairs in a single experiment. These outer capsule liquids were always higher in carbon than the inner capsules, but these two cases are reported to supplement the number of complete liquid–solid pairs. Measured carbon contents in all liquids, including those in the outer capsules, were a factor of 5–10 lower than those reported by Gaetani & Grove (1998) (Fig. 4).

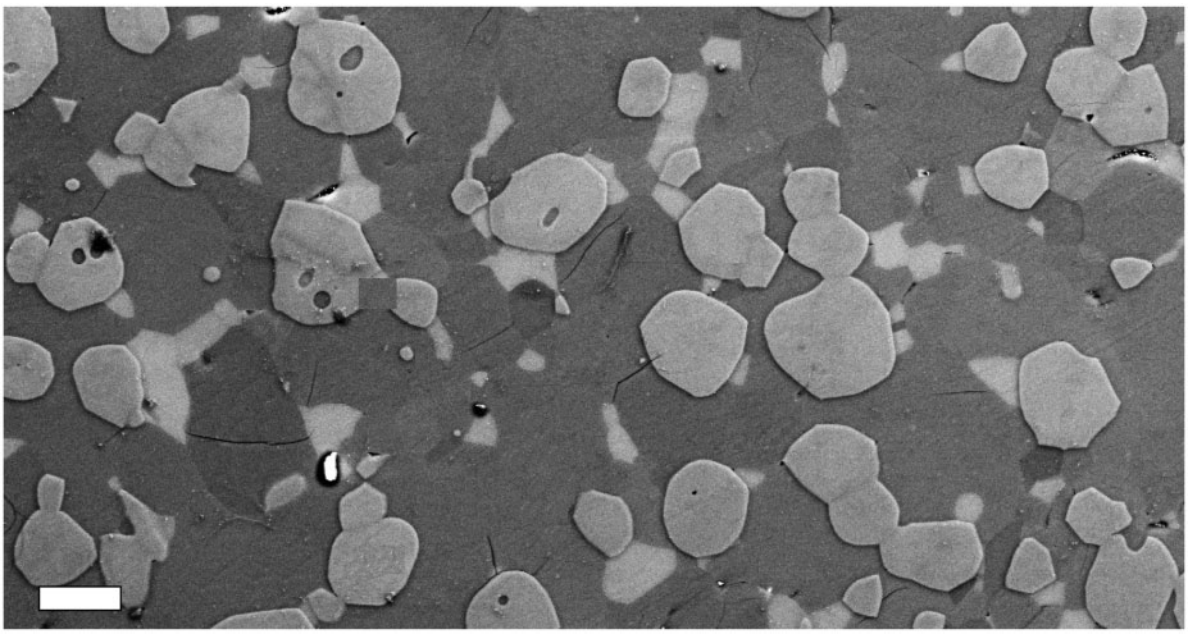

Fig. 2. Backscattered electron image of a polished section of a typical recrystallized peridotite. High relief, bright grains are garnet, lower relief light colored grains are cpx, and the darker matrix is composed of olivine grains. Scale bar represents 10 μm.

Experiments contained large amounts of measurable, homogeneous silicate glass (Fig. 3), in pools up to ~500 μm in diameter. Melt wetted most crystal surfaces, giving opportunity for full reaction of the liquid with the solids. Solids always sank to the bottom of each capsule regardless of loading configuration. The run products showed substantial modification on quench. Virtually all the solid grains had an iron-rich quench rim 1–3 μm thick that was avoided during microprobe analysis; no other zonation was observed or measured. Interstitial liquid occasionally formed quench needles, and was always depleted in MgO and FeO compared with the large melt pool. Elongate quench needles were common at the boundary between solids and liquids. The boundary between the capsule walls and the liquid pool commonly showed quench crystallization of 10–100 μm pargasitic amphibole of a composition close to the unmodified glass. In all cases, these quench features were avoided for analyses. In some samples, 100 nm scale phases were observed visually within the glass pools, presumably also formed on quench. However, these phases were much smaller than the activation volume of the electron probe or the wavelength of the IR radiation, and no obvious change was observed in compositions between areas with and without those phases. The assumption of homogeneous glass is therefore probably adequate.

Approach to equilibrium

Establishment of equilibrium in this type of melting experiment is difficult, as an appropriate method of reversal has not been devised. Several techniques suggest that our experiments either achieved liquid–solid equilibrium or were very close. First, measured values of the olivine-liquid K_D parameter were between 0·32 and 0·40, most consistently 0·35–0·36. The calibration of Toplis (2005) predicts a K_D of ~0·36 at these liquid compositions, with K_D increasing as H_2O content decreases. Our measured K_D values are consistent with those reported by Gaetani & Grove (1998) for their hydrous experiments at lower temperatures and pressures, and are generally within the range deemed acceptable by Toplis (2005). Two samples have high K_D values (0·38 and 0·40), potentially reflecting either disequilibrium between the liquid and the solids owing to Fe loss to the capsules or slight changes in the Fe–Mg distribution on quench. However, the difference in liquid composition is small and confined to Fe and Mg, which will be treated together, and therefore the data for these experiments are still included here. These two samples would require a loss of less than 10% of the available Fe in the liquid to the capsule to be consistent with the other measured K_D values.

Iron contents vary between experiments owing to the initial compositions of the liquids and the Fe-doped capsules. The glass used in the final set of experiments was higher in Fe than the final composition, necessitating some loss of iron to either diffusion into the capsule or crystallization of the solids. For the initial experiments, the capsules buffered the iron content at a higher level than predicted; this produced olivines with Mg-number 86–87 and liquids with lower MgO contents than would be

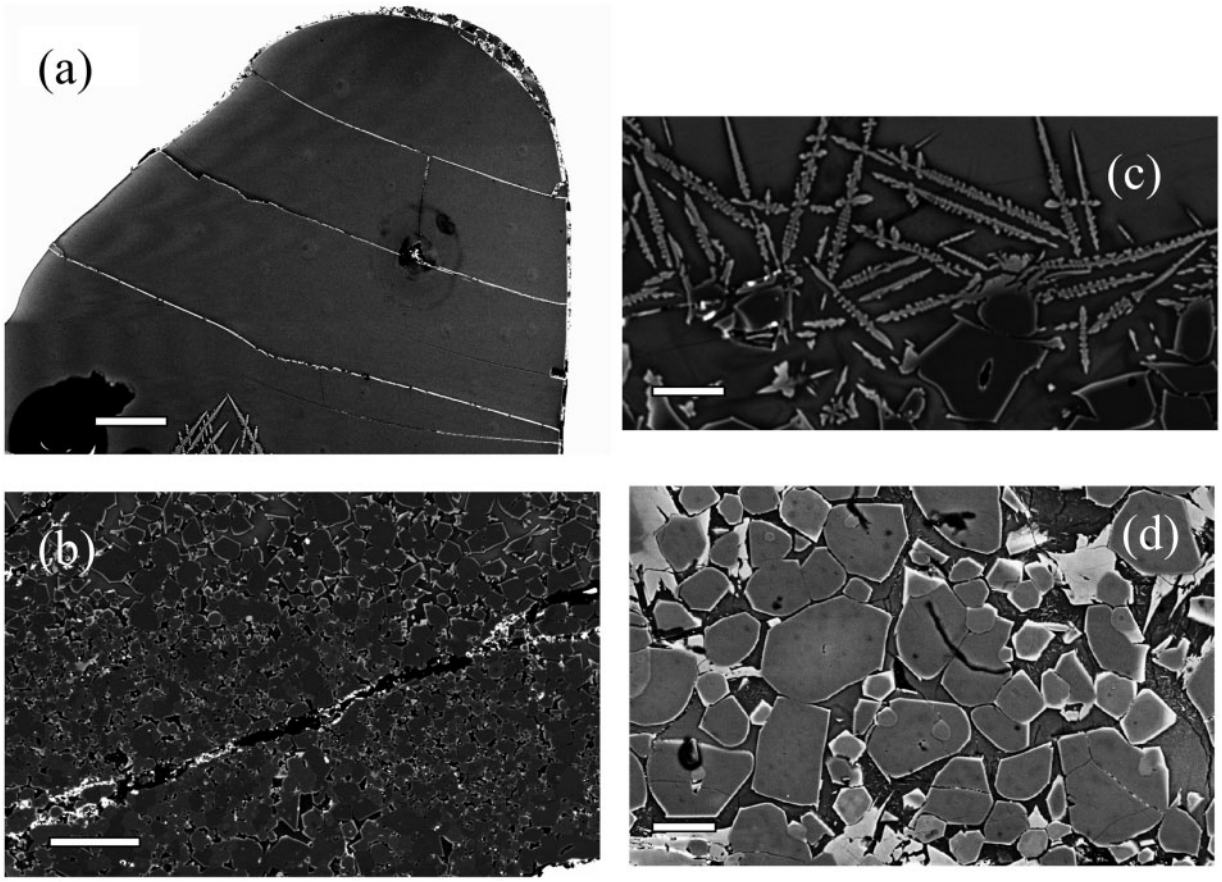

Fig. 3. Backscattered electron images of experimental run products. (a) Melt pool at the top of R380. Some quench needles can be seen at the bottom of the image, along with several spots showing polishing or probe-beam damage. The AuPd capsule is bright white in this image. Circular features are polishing damage; they were confirmed not to be vesicles by optical examination. (b) Solid pile from the bottom of the same run. Dark crystals are olivine, lighter crystals are garnet and cpx. Bright rims around most grains are quench features. Dark, interstitial material is glass or partly crystalline groundmass that has lost much of its MgO, FeO, and often CaO to the quench boundaries on the grains. Horizontal elongate features are cracks formed on quench. (c) Close-up view of the quench needle texture, also showing solid grains with homogeneous cores and quench-growth rims. (d) Solid crystals showing lack of significant zoning other than due to quench effects. Scale bars in (a) and (b): 100 μm; scale bars in (c) and (d): 30 μm.

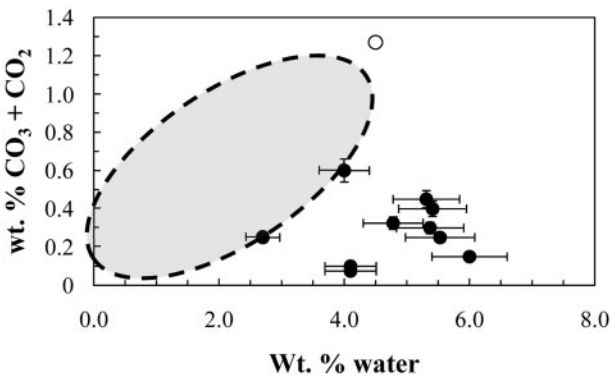

Fig. 4. Measured volatile contents for our experiments (filled circles) compared with the volatile contents of Gaetani & Grove (1998) (open circle) and the field of volatile contents (ellipse) from the experiments of Liu *et al.* (2006).

expected in actual mantle liquids. New capsules were then prepared with less Fe to equilibrate with a lower-iron liquid composition; these liquids equilibrated with Mg-number 88–90 olivine, close to the expected mantle value. Measured liquid and solid compositions are given in Table 2.

Three additional lines of evidence suggest close approach to equilibrium. Typically, Fe–Mg zoning, which would be expected in the case of significant Fe loss or gain, is easily seen in electron microprobe transects across single grains or in back-scattered electron (BSE) images. In our experiments, zoning is typically only barely visible in BSE (Fig. 3) and measurements of solid compositions from cores and rims of grains are indistinguishable if obvious quench features are avoided. A lack of clear zoning has been taken previously as evidence for close approach to equilibrium (Parman & Grove, 2004). If our

Table 2: Full experimental results; compositions given in weight per cent

Run no.:	R389				R385			
Phase:	Liq	Ol	Gt	CPX	Liq	Ol	Gt	CPX
SiO_2	45·29(26)	40·73(42)	42·12(15)	53·08(7·2)	45·38(29)	40·86(12)	42·09(18)	53·09(53)
TiO_2	0·68(1·8)	0·00(3·1)	0·16(0·9)	0·13(0)	0·80(2·4)	0·00(0·5)	0·28(6·6)	0·23(9·5)
Al_2O_3	13·0(10)	0·03(35)	22·24(46)	5·19(1·0)	12·71(10)	0·05(1·8)	22·91(22)	5·79(43)
FeO	8·05(12)	10·91(82)	8·01(59)	4·41(32)	9·12(12)	11·35(28)	9·25(59)	4·34(29)
MnO	0·15(0·7)	0·13(0·8)	0·24(0·3)	0·11(0·2)	0·15(0·6)	0·13(0·5)	0·24(0·9)	0·10(0·7)
MgO	14·09(24)	47·80(96)	19·28(43)	18·04(18)	13·40(7·9)	47·71(59)	18·76(70)	17·24(70)
CaO	9·70(6·3)	0·17(46)	6·47(81)	17·03(0·8)	9·05(6·2)	0·23(2·4)	6·13(38)	17·44(76)
Na_2O	2·46(10)	0·00(3·7)	0·03(6·7)	1·10(0·2)	3·23(10)	0·02(0·3)	0·04(1·1)	1·87(14)
K_2O	0·38(3·1)	0·00(0·2)	0·00(0·5)	0·00(0·2)	0·49(2·7)	0·00(0·3)	0·00(0·2)	0·00(0·6)
NiO	0·01(1·8)	0·01(0·9)	0·00(0·2)	0·00(0·7)	0·00(1·8)	0·02(0·8)	0·00(0·6)	0·00(0·7)
Cr_2O_3	0·14(3·7)	0·06(31)	1·23(1·6)	0·49(0·9)	0·08(2·7)	0·02(1·9)	0·33(18)	0·22(21)
P_2O_5	0·00(1·1)	0·00(0·6)	0·00(0·1)	0·00(0·1)	0·00(0·7)	0·00(0·6)	0·00(0·8)	0·01(0·7)
Oxide totals	94·02(25)	99·88(31)	99·84(18)	99·63(14)	95·38(45)	100·44(26)	100·08(27)	100·40(43)
Mg-no.	0·757	0·886	0·810	0·880	0·724	0·882	0·783	0·872
K_D		0·399				0·350		
H_2O	6				5·53			
CO_3	0·15				0·24			
Liquid totals	100·18				101·16			
Run duration (h)	16				19			

Run no.:	R390				R395			
Phase:	Liq	Ol	Gt	CPX	Liq	Ol	Gt	CPX
SiO_2	43·77(19)	40·81(13)	41·84(29)	53·36(37)	45·47(33)	41·36(13)	42·55(28)	53·58(21)
TiO_2	0·72(2·1)	0·00(0)	0·21(3·1)	0·12(1·1)	0·69(1·1)	0·00(0·4)	0·23(0·0)	0·10(8·3)
Al_2O_3	12·52(12)	0·04(1·8)	22·44(19)	5·35(17)	12·57(13)	0·26(10)	22·92(31)	5·08(19)
FeO	10·36(11)	12·30(36)	10·71(68)	4·39(33)	7·24(12)	9·66(42)	8·21(82)	4·11(38)
MnO	0·16(0·5)	0·13(0·7)	0·23(0·9)	0·10(0·7)	0·14(0·5)	0·12(0·3)	0·22(0·5)	0·10(0·9)
MgO	13·43(6·8)	47·07(19)	17·21(48)	17·56(13)	14·47(13)	48·84(12)	19·57(17)	19·03(39)
CaO	9·85(6·7)	0·17(1·9)	6·99(34)	17·95(54)	9·49(9·1)	0·31(30)	6·28(14)	16·05(26)
Na_2O	2·78(14)	0·01(0·4)	0·02(0·3)	1·43(2·4)	2·69(12)	0·01(3·9)	0·02(0·3)	1·39(0·7)
K_2O	0·44(1·6)	0·00(0)	0·00(0·3)	0·00(0·3)	0·37(1·9)	0·00(0·2)	0·00(0)	0·00(0·1)
NiO	0·02(2·1)	0·03(1·2)	0·00(0·4)	0·00(0·3)	0·00(0·9)	0·04(0·9)	0·00(1·2)	0·00(0·6)
Cr_2O_3	0·10(1·9)	0·03(0·7)	0·87(12)	0·36(7·8)	0·12(1·1)	0·04(7·3)	0·68(1·5)	0·51(10)
P_2O_5	0·01(1·2)	0·00(0·1)	0·01(0·9)	0·01(0·6)	0·01(1·1)	0·00(0·5)	0·00(0·9)	0·01(0·7)
Oxide totals	94·28(22)	100·64(8)	100·58(23)	100·68(16)	93·31(57)	100·67(49)	100·74(22)	100·01(23)
Mg-no.	0·698	0·872	0·741	0·877	0·781	0·900	0·809	0·892
K_D		0·339				0·383		
H_2O	5·37				5·31			
CO_3	0·284				0·45[1]			
Liquid totals	99·94				99·08			
Run duration (h)	18				6			

(continued)

Table 2: Continued

Run no.:	R396				R398			
Phase:	Liq	Ol	Gt	CPX	Liq	Ol	Gt	CPX
SiO_2	43·69(27)	40·41(23)	41·91(21)	52·96(40)	44·69(53)	40·42(25)	41·63(58)	53·01(40)
TiO_2	0·74(2·5)	0·00(0·5)	0·17(1·1)	0·12(1·8)	0·67(6·2)	0·00(1·1)	0·20(0·0)	0·10(1·8)
Al_2O_3	13·01(13)	0·07(6·4)	23·01(16)	5·81(8·7)	12·47(11)	0·03(6·3)	22·75(1·8)	5·07(14)
FeO	8·66(16)	10·78(52)	8·13(17)	4·60(11)	8·56(12)	9·51(26)	8·24(23)	4·31(12)
MnO	0·14(0·8)	0·12(1·0)	0·23(1·9)	0·09(0·8)	0·15(0·6)	0·12(0·7)	0·22(0·9)	0·09(0·7)
MgO	13·95(33)	48·22(53)	20·43(26)	18·16(15)	14·81(34)	50·14(21)	20·51(54)	18·74(29)
CaO	9·52(20)	0·27(16)	6·26(34)	16·93(7·5)	9·52(23)	0·20(51)	6·55(3·3)	17·27(9·0)
Na_2O	2·86(1·1)	0·01(0·6)	0·01(2·3)	1·21(6·6)	2·76(1·1)	0·00(4·8)	0·02(0·6)	1·25(20)
K_2O	0·34(0·2)	0·00(0·1)	0·00(0·3)	0·00(1·4)	0·43(0·3)	0·00(0·3)	0·00(0)	0·00(4·4)
NiO	0·00(1·7)	0·05(1·4)	0·00(0·8)	0·00(1·3)	0·00(1·8)	0·01(1·4)	0·01(1·4)	0·01(1·5)
Cr_2O_3	0·09(10)	0·03(0·8)	0·80(15)	0·43(1·3)	0·12(12)	0·06(11)	0·64(0·9)	0·34(1·5)
P_2O_5	0·01(0·5)	0·00(1·1)	0·00(1·1)	0·01(2·0)	0·01(0·9)	0·00(0·7)	0·01(0·7)	0·02(1·3)
Oxide totals	93·07(34)	100·02(10)	101·00(22)	100·38(60)	94·23(83)	100·54(45)	100·83(107)	100·27(59)
Mg-no.	0·742	0·889	0·817	0·875	0·755	0·904	0·816	0·886
K_D		0·360				0·328		
H_2O	4·78				5·41			
CO_3	0·325				0·38			
Liquid totals	98·18				100·03			
Run duration (h)	8				9			

Run no.:	R380IC[2]			R380OC[2]			
Phase:	IC Liq	IC Ol	IC GT	OC Liq	OC Ol	OC Gt	OC CPX
SiO_2	44·11(26)	40·51(35)	41·60(27)	44·64(19)	40·73(45)	42·11(43)	52·91(10)
TiO_2	0·54(0·3)	0·00(5·4)	0·22(2·2)	0·64(0·3)	0·00(9·3)	0·20(2·1)	0·10(2·7)
Al_2O_3	11·61(24)	0·11(40)	22·60(12)	12·41(2·4)	0·06(62)	21·96(23)	5·52(9·9)
FeO	11·5(32)	12·76(81)	9·48(22)	9·44(27)	10·40(48)	7·69(21)	4·37(18)
MnO	0·12(1·3)	0·10(1·7)	0·20(1·4)	0·14(0·8)	0·11(1·4)	0·21(1·6)	0·10(2·2)
MgO	15·15(56)	46·35(78)	19·18(16)	14·56(22)	48·18(54)	20·30(19)	18·79(39)
CaO	8·11(3·2)	0·18(59)	5·68(12)	9·30(1·7)	0·20(41)	6·17(25)	15·96(12)
Na_2O	2·47(0·8)	0·01(1·1)	0·02(9·9)	2·83(1·0)	0·01(3·8)	0·04(3·9)	1·17(11)
K_2O	0·23(0·2)	0·00(0·3)	0·00(1·9)	0·32(0·3)	0·00(0·2)	0·00(0·4)	0·00(1·4)
NiO	0·01(2·0)	0·05(1·6)	0·01(1·6)	0·00(1·3)	0·03(1·2)	0·00(0·8)	0·00(0·5)
Cr_2O_3	0·15(1·6)	0·06(20)	0·60(1·8)	0·11(0·7)	0·04(23)	0·67(9·7)	0·49(1·4)
P_2O_5	0·01(0·7)	0·00(0·9)	0·00(1·5)	0·00(1·0)	0·00(0·9)	0·01(1·2)	0·01(3·2)
Oxide totals	94·13(54)	100·17(37)	99·64(41)	94·46(52)	99·82(31)	99·41(45)	99·48(52)
Mg-no.	0·705	0·866	0·782	0·734	0·892	0·824	0·885
K_D		0·361			0·333		
H_2O	2·7			4			
CO_3	0·24			0·61			
Liquid totals	97·08			99·07			
Run duration (h)	15			15			

(continued)

Table 2: Continued

Run no.:	R393IC[2]			R393OC[2]			
Phase:	IC Liq	IC Ol	IC Gt	OC Liq	OC Ol	OC Gt	OC CPX
SiO_2	43·67(30)	40·52(24)	42·15(22)	44·37(18)	40·76(10)	42·11(13)	52·96(7·0)
TiO_2	0·59(0·6)	0·00(3·3)	0·14(4·2)	0·72(1·1)	0·00(0·2)	0·21(5·0)	0·13(1·0)
Al_2O_3	11·91(8·6)	0·08(25)	22·60(20)	12·75(11)	0·05(0·8)	22·91(7·4)	5·57(8·1)
FeO	11·30(17)	12·95(48)	8·70(34)	8·58(13)	10·76(14)	7·85(38)	4·18(15)
MnO	0·15(1·5)	0·11(1·7)	0·20(2·2)	0·15(0·6)	0·12(0·1)	0·22(0·8)	0·10(0·6)
MgO	13·26(54)	46·62(53)	20·06(61)	14·06(8·6)	48·63(23)	19·89(43)	18·58(19)
CaO	8·83(3·9)	0·20(40)	5·27(34)	9·34(6·5)	0·21(4·2)	6·13(21)	16·64(14)
Na_2O	2·47(0·8)	0·01(1·2)	0·01(10·0)	2·87(7·7)	0·01(0·6)	0·01(0·8)	1·26(3·9)
K_2O	0·26(0·4)	0·00(0·3)	0·00(2·2)	0·38(1·3)	0·00(0·2)	0·00(0·2)	0·00(0·3)
NiO	0·02(2·3)	0·04(0·9)	0·00(2·7)	0·02(1·6)	0·03(1·0)	0·00(0·6)	0·01(1·0)
Cr_2O_3	0·15(2·1)	0·07(24)	1·05(3·2)	0·10(2·8)	0·03(0·6)	0·60(14)	0·31(8·1)
P_2O_5	0·01(1·0)	0·00(1·1)	0·01(1·6)	0·01(1·8)	0·01(0·2)	0·01(0·7)	0·01(0·9)
Oxide totals	92·68(47)	100·66(37)	100·25(56)	93·39(22)	100·65(24)	100·00(16)	99·82(18)
Mg-no.	0·676	0·865	0·804	0·745	0·890	0·819	0·888
K_D		0·326			0·362		
H_2O	4·1			4·1			
CO_3	0·075			0·105			
Liquid totals	96·86			97·60			
Run duration (h)	12			12			

[1]Includes 0·13 wt % molecular CO_2.
[2]Two experiments lack cpx analyses; the cpx grains available were too small to obtain electron probe analyses not contaminated by the exterior quench layer. In these cases, the three major phases and liquid compositions were also measured in the outer capsule, and inner capsule (IC) and outer capsule (OC) groupings are noted, as described in text.
[3]Values in parentheses are 100 × the standard deviation of the electron microprobe measurements.
[4]Analyses are averages of >5 grains per sample, typically 10–20 grains, with 1–3 points per grain as size allowed.
[5]All inner capsules were prepared with ~1 mg of garnet peridotite (Table 1), 1 mg NX-08 (Table 1), and excess water. Water contents always decreased from starting conditions, most probably because of water loss while arc-welding small capsules.

experiments were far from equilibrium, significant zoning would be expected as the solid compositions shift substantially during the run (see below). Additionally, as Ni was found to be compatible in our capsules and the minerals in our garnet peridotite starting material contained nickel, measuring grains with significant Ni contents would suggest incomplete reaction. Significant Ni contents were not observed at the detection limit of the electron microprobe (Table 2), suggesting full equilibration for this component on the timescale of the experiments. Finally, experiments were run with durations of 6–20 h, with no increase in mineral zoning in the short experiments, suggesting that solid equilibration is rapid relative to the timescales of the experiments. Although these experimental timescales are short compared with other studies (e.g. Walter, 1998; Parman & Grove, 2004) the small grain sizes and high water contents probably promoted fast reaction between the solid and liquid assemblages, allowing for a close approach to equilibrium.

FTIR results

Volatile contents measured by FTIR combined with electron probe totals typically gave totals that were 98% or better. Mismatch decreased in the samples with lower measured water contents. Typical water-containing glass IR spectra are displayed in Fig. 5. Significant and unexpected band structure was observed. We report the first analyses of water-containing glasses that show the 4500 cm^{-1} band split into a triplet. In basaltic liquids, a single peak near 4500 cm^{-1} is common, and a small shoulder is occasionally observed (S. Newman, personal communication, 2009). Withers *et al.* (2009) also reported FTIR spectra of experimentally produced basaltic glasses showing a doublet, but there are no previous reports of a

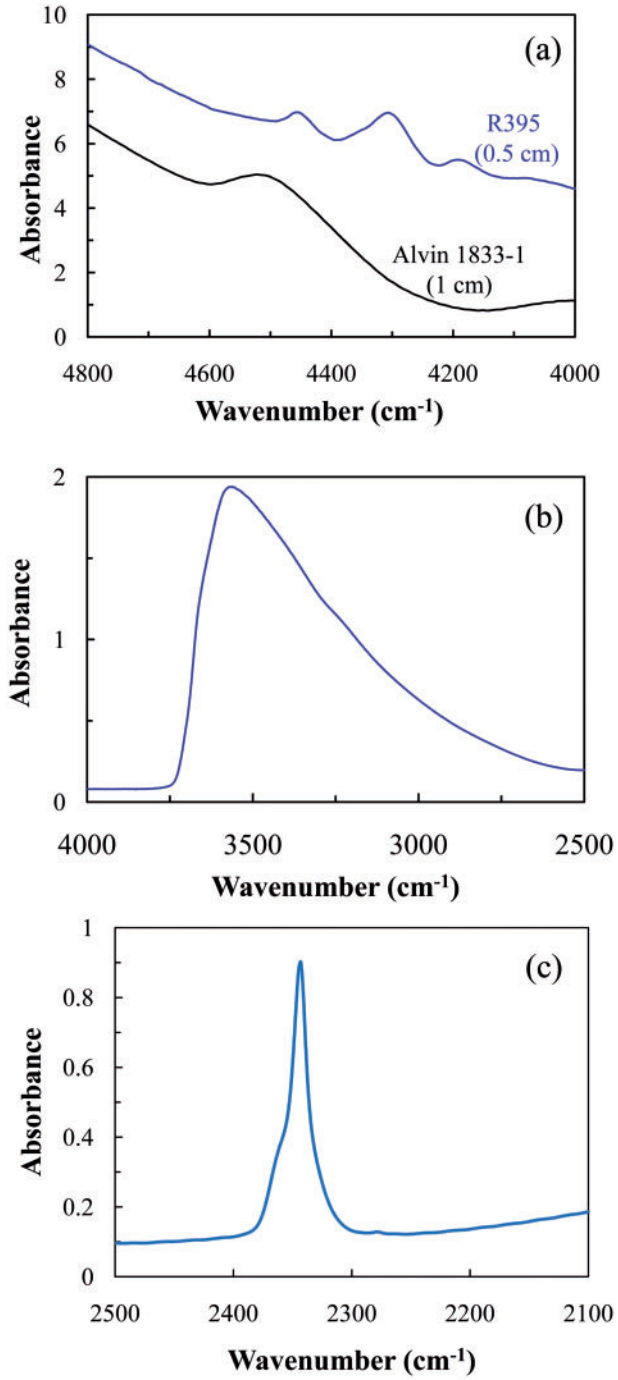

Fig. 5. Representative FTIR spectra of glasses. (a) The characteristic structure seen in our near-IR spectra (sample R395, upper spectrum) and a more typical spectrum of a hydrous basalt [sample Alvin 1833-1 of Stolper & Newman (1994); lower spectrum]; (b) 3600 cm^{-1} water band from sample R393, thinned down to ~54 μm to bring the peak on scale; (c) measurable molecular CO_2 peak from R395, the only sample with a large molecular CO_2 peak.

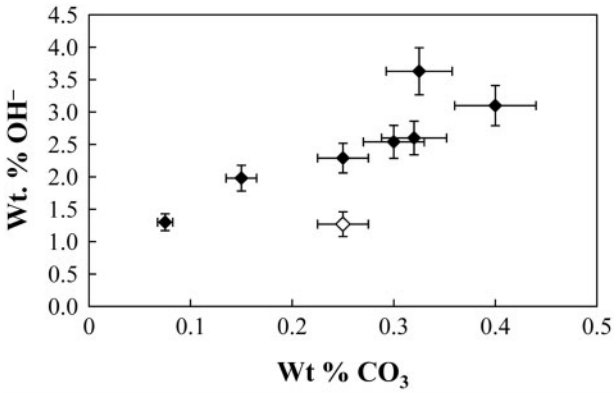

Fig. 6. Correlation between OH^- content and carbonate content (wt %) as measured by FTIR. R380 (open symbol) falls off the trend as it is the lowest total water content sample and probably is not saturated fully in OH^-.

triplet in this region. We hypothesize that the 4500 cm^{-1} peak splits into multiple peaks in our experiments because of interactions between the Si–O–H groups and other components in the melt. In some minerals, this region of the IR spectrum shows complexity owing to bonding between the OH^- groups and other elements such as Fe, Al, and Mg (e.g. Bishop *et al.*, 2002). Interaction of carbonate, H_2O, and OH^- groups in glasses could also produce changes in the IR spectra. Our composition differs from previously analyzed basalts, which are generally fractionated and degassed before eruption (Dixon *et al.*, 1995). For instance, the higher MgO and carbonate contents might be the cause of the unusual band structure.

We observed a relationship between water speciation and carbonate concentration in the glass. The 4500 cm^{-1} peak amplitude, proportional to OH^- concentration, increases with increasing carbonate content among our experiments (Fig. 6). This suggests that reaction with carbonate creates additional bridging oxygens that in turn react with water to give additional hydroxyl groups. This interaction may explain a portion of the IR band splitting. The lowest water-content sample, R380, falls off this trend, perhaps because it is not saturated in OH^-. Dixon *et al.*, (1995) showed that ~4 wt % H_2O is required to saturate a basaltic liquid in OH^-. The remaining liquids have higher water contents, may be saturated in OH^-, and may better demonstrate the interaction between the water and carbonate species.

Another unexpected observation in the IR spectra is the presence of a molecular CO_2 band near 2340 cm^{-1} in three of our samples. Two experiments showed small molecular CO_2 contents above the background and one sample, R395, showed a larger band (Fig. 5). Typically, molecular CO_2 is observed only in liquids with higher SiO_2 contents, as the molecular CO_2 is expected to react with non-bridging oxygen atoms to produce bridging oxygen

atoms and carbonate groups (e.g. Dixon *et al.*, 1995; Liu *et al.*, 2006). Because this species has not been previously observed in basalts, the absorption coefficient has not been determined. We used use the calibration of Morizet *et al.* (2002) for a phonolitic melt as it was the lowest absorption coefficient we could find, offering a conservatively high estimate for our CO_2 concentrations. Even using this calibration, the molecular CO_2 contents for R398 and R385 were less than 0·01 wt %. However, R395 was estimated to have 0·14% molecular CO_2. R395 is not unusual in its liquid composition, water content, or total carbon content compared with the other samples in this study, and so this molecular CO_2 is difficult to explain. Several workers have hypothesized that speciation of carbon in quenched glasses may not always be representative of the high-temperature speciation. In particular, Morizet *et al.* (2001) argued that molecular CO_2 may be more abundant at high temperatures than in typical quenched glasses. If so, the presence of molecular CO_2 in these samples may reflect a particularly rapid quench. However, it is equally possible that molecular CO_2 in these samples could reflect a slower quench that allowed for conversion of carbonate to molecular CO_2, and we see no way to distinguish between these possibilities based on the current experiments.

DISCUSSION

Previous work provides a framework for evaluating our liquid and solid compositions. Anhydrous experiments from 3 to 7 GPa on fertile peridotites by Walter (1998) have served as the basis for analysis of melting at these pressures (e.g. Humayun *et al.*, 2004; Herzberg, 2006). Longhi (2002) produced anhydrous melting experiments from 2·4 to 3·4 GPa with similar compositions to those reported by Walter (1998), used those experiments as the basis for creating the empirical BATCH calculator, and applied the calculation to anhydrous peridotite melting under similar conditions. Gaetani & Grove (1998) produced hydrous, carbon-containing liquids at lower pressures, from 1·2 to 2 GPa. All these experiments and the calculated liquid composition from pHMELTS are used to place our results in context. Following the approach of Gaetani & Grove (1998), we discuss the liquids both on a renormalized volatile-free basis, for direct comparison with volatile-free experiments, and on a hydrous basis to better constrain the underlying thermodynamics and element partitioning. An average composition, based on our experiments, that should be in equilibrium with Mg-number ~89 olivine is given in Table 3, normalized to a 100% total. Also given are liquids from the closest temperature and pressure conditions available from the other four studies mentioned above. The pHMELTS algorithm calculates a liquid that is vastly over-enriched in Na_2O, as discussed below, necessitating care when making inferences using single oxide compositions; ratios of one oxide to another and normative mineral components will be considered subsequently as, in many cases, these quantities are more robust (except those involving Na_2O). Volatile-free liquid compositions from these studies are displayed graphically in Fig. 7, which plots each of the major oxides in a form similar to trace element variation diagrams, showing the differences in liquid compositions on a single chart and facilitating comparison of single oxide abundances.

Table 3: Average hydrous liquid composition from this study compared with other experimental and calculated liquids

	This work		pHMELTS	Longhi[1]	Walter[2]	Gaetani & Grove[3]
	Hydrous	Volatile-free				
SiO_2	44·56	47·42	42·44	45·60	46·17	43·88
Al_2O_3	12·60	13·41	8·97	15·10	13·32	15·41
CaO	9·40	10·01	3·00	6·91	10·69	10·2
MgO	14·01	14·91	15·58	15·30	16·90	13·36
FeO	9·04	9·62	9·59	9·60	9·55	8·21
Na_2O	2·78	2·96	15·03	2·68	0·96	2·2
K_2O	0·38	0·41	0·00	2·13	0·56	0·1
MnO	0·15	0·12	0·00	0·21	0·18	0·12
TiO_2	0·90	0·96	1·16	1·43	0·91	0·64
Cr_2O_3	0·12	0·12	1·61	0·22	0·31	0·15
H_2O	4·95		2·56			5·3
CO_3	0·10					1·25

[1]Calculated 1% melt of PUM at 3 GPa from Longhi (2002).
[2]Experiment 30.12, the lowest-temperature liquid composition given from 3 GPa, although the solid assemblage for this sample did not include garnet; 3 GPa, 1515°C.
[3]Experiment B365; 2 GPa, 1290°C.

MgO, FeO, SiO_2

The effect of H_2O addition on the MgO + FeO and SiO_2 contents of silicate melts has been a major source of controversy since it was proposed that direct hydrous melting of peridotite can produce high-silica, andesitic melts from the mantle (e.g. Kushiro, 1972). Gaetani & Grove (1998) proposed that addition of water moves the liquid from olivine-normative to quartz-normative by decreasing the $(XMgO + XFeO)/XSiO_2$ ratio. Increasing H_2O results in a slight decrease in liquid SiO_2 content in the nominal analysis, but renormalization to an anhydrous basis gives the opposite trend, with increasing SiO_2. Based on a simplified system, Liu *et al.* (2006) confirmed that the MgO/SiO_2 ratio decreases in hydrous liquids entirely as a result of decreasing MgO at nearly constant SiO_2. Whereas

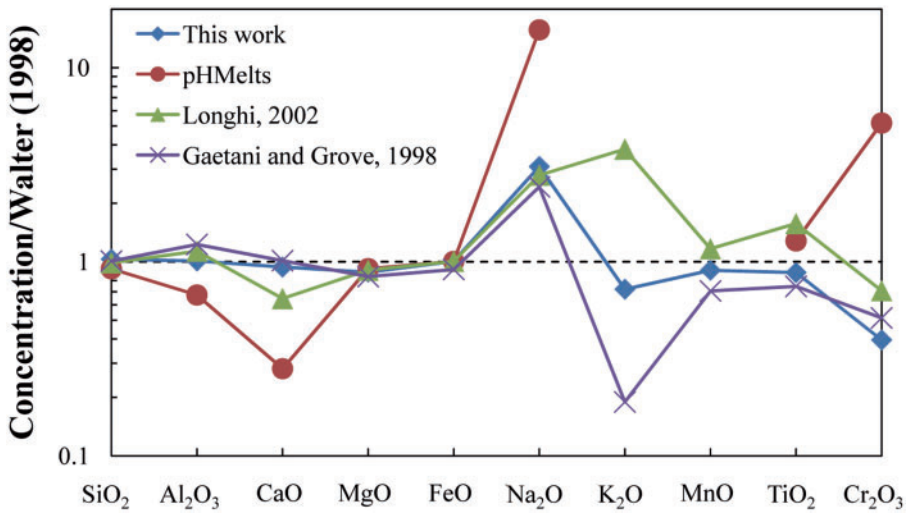

Fig. 7. Concentration in experimental liquids normalized to experiment 30.12 of Walter (1998), with the dashed line marking that study. pHMelts cannot include MnO or K_2O effectively, so those two oxides were not included in the calculation and their values are not plotted.

their system was Fe-free, our liquids contain both MgO and FeO—both major components of olivine—and thus we will consider these oxides jointly. The pHMELTS algorithm calculates a hydrous liquid with a much lower SiO_2 content than our liquid and the highest $(XMgO + XFeO)/XSiO_2$ ratio of any near-solidus liquid considered here (Table 3).

Comparison with anhydrous liquids from the 3 GPa experiments of Walter (1998) and Longhi (2002) shows that our experiments have less SiO_2 when considered on a hydrous basis (Fig. 8). Renormalized to volatile-free totals, however, the SiO_2 of our liquids is higher than in the anhydrous liquids, consistent with the description of Gaetani & Grove (1998). In fact, the SiO_2 contents of the liquids are similar to or higher than those measured by Gaetani & Grove (1998), which is surprising as most of their experiments contain opx and the silica activity fixed by the opx–olivine equilibrium shifts to lower values with increasing pressure (e.g. Ghiorso *et al.*, 1983). Our experiments lack opx, and so should lie at a lower SiO_2 activity than the opx–olivine buffer. Liu *et al.* (2006) noted a correlation between increasing Na_2O in their liquids and increasing silica content, and Na_2O is known to reduce the silica activity coefficient (Hirschmann *et al.*, 1998). Our liquids do contain higher Na_2O than those in Gaetani & Grove (1998); however, a more likely explanation is the presence of carbon, as Liu *et al.* (2006) also noted that CO_3^{2-} counteracts some of the effect of water in silicate liquids. The high carbon contents in the experiments of Gaetani & Grove (1998) could have driven their liquids to lower SiO_2 through this interaction, whereas our liquids are much lower in CO_3^{2-} and thus retain the increased SiO_2 owing to the effects of water. Similarly,

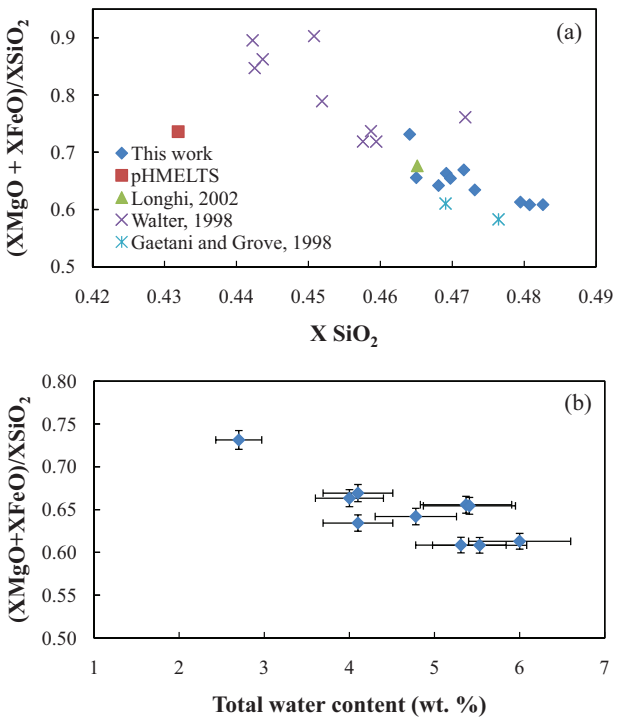

Fig. 8. (a) Molar $(MgO + FeO)/SiO_2$ as a function of $XSiO_2$. Shown in addition to our data are all data points from 3 to 4 GPa of Walter (1998), the two 2 GPa experiments of Gaetani & Grove (1998), the 1% melt of primitive upper mantle (PUM) at 3 GPa of Longhi (2002), and the calculated hydrous melt from pHMELTS. Errors on our experiments in (a) are about the size of the symbols. (b) shows the correlation in our samples between increasing water content and decreasing $(X_{MgO} + X_{FeO})/X_{SiO2}$.

compared with the calibration of Wood & Turner (2009) for the effect of water on lherzolite melt composition, our liquids are higher in SiO_2 than expected for the measured water content, which we again attribute most probably to the presence of carbon in previous studies.

The MgO content of our liquids can be understood in a similar fashion, in particular when both the MgO and FeO of the liquid are considered as normative olivine, with the FeO fixed by the composition of the capsule materials. Compared with the 3 GPa liquids of Walter (1998), Longhi (2002), and that calculated by pHMELTS, our hydrous liquids are lower in $(MgO+FeO)/SiO_2$ (Fig. 8), whereas compared with the lower pressure experiments of Gaetani & Grove (1998), our liquids have higher $MgO+FeO$ contents at similar SiO_2, owing to the well-established shift in the near-solidus liquid composition towards olivine with increasing pressure (Longhi, 2002). Gaetani & Grove (1998) also drew correlations between the olivine/liquid D_{MgO}, D_{FeO}, and temperature, covering both their hydrous experiments and those of Kinzler & Grove (1992). The pHMELTS model predicts D_{MgO} and D_{FeO} close to their trend. However, our olivine/liquid D_{MgO} and D_{FeO} are consistently higher than those predicted by the correlation with temperature (Fig. 9). As with the change in SiO_2, this increase in D_{MgO} and D_{FeO} is a function of liquid composition, most probably owing to the presence of carbon in their experiments.

An alternative and equivalent explanation for the MgO–FeO–SiO_2 systematics is that addition of water to the liquid expands the stability field of olivine relative to the other phases (Fig. 10). Longhi (2002) showed that the melt in equilibrium with a full peridotite assemblage increases in olivine component with increasing pressure. Addition of water decreases $(MgO+FeO)/SiO_2$ and moves the liquid composition away from olivine (Fig. 10). Adding water to a silicate liquid depolymerizes the liquid; bridging oxygen atoms are separated by reaction with water to produce OH^- groups. This effect qualitatively makes the liquid more 'olivine-like', in the sense that the olivine structure contains no bridging oxygens and would be considered fully depolymerized. During low-pressure crystallization, the effect of water is well established: increased water content causes additional crystallization of olivine relative to other phases (e.g. Asimow *et al.*, 2004). A rigorous explanation of these relationships would require detailed understanding of the relationship between liquid speciation and component activities, but qualitatively, making a liquid structurally more like olivine has a similar effect on liquidus relations to making a liquid compositionally more like olivine, bringing it closer to the olivine liquidus field.

The liquid calculated by the pHMELTS algorithm misses the effect of water on the $(MgO+FeO)/SiO_2$ ratio by the largest amount. The calibration includes few constraints on hydrous phase relations at high pressure and does not consider CO_3^{2-}, which appears to exert a strong influence.

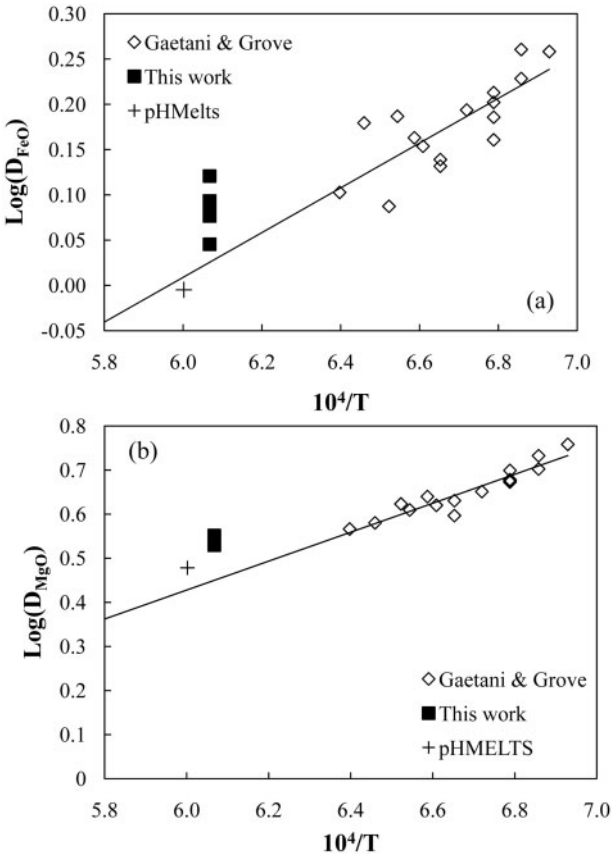

Fig. 9. Olivine/liquid partition coefficients as a function of inverse correlation of Gaetani & Grove (1998) compared with our data and the hydrous melt composition from pHMELTS. (a) D_{FeO}; (b) D_{MgO}.

Al_2O_3

On a volatile-free basis, the Al_2O_3 content of our liquid appears to be controlled by the presence of garnet. Although our starting peridotite was over-enriched in Al_2O_3 during grinding, this enrichment does not appear to have resulted in an increased liquid Al_2O_3, and multiple saturation was still achieved. To confirm the validity of these experiments, first we compare our Al_2O_3 abundances with other studies. Although not all of the experiments of Walter (1998) contained garnet, and no single experiment at 3 GPa reported analyses of both garnet and liquid, our liquid is similar in Al_2O_3 content to the 3 GPa liquids of Walter (1998). Compared with the experiments of Gaetani & Grove (1998), which were all either within the spinel lherzolite stability field or close to the spinel-to-garnet transition, our liquid is substantially lower in Al_2O_3, despite the added Al_2O_3 in our experiments. These comparisons suggest first that the additional Al_2O_3 increases the modal

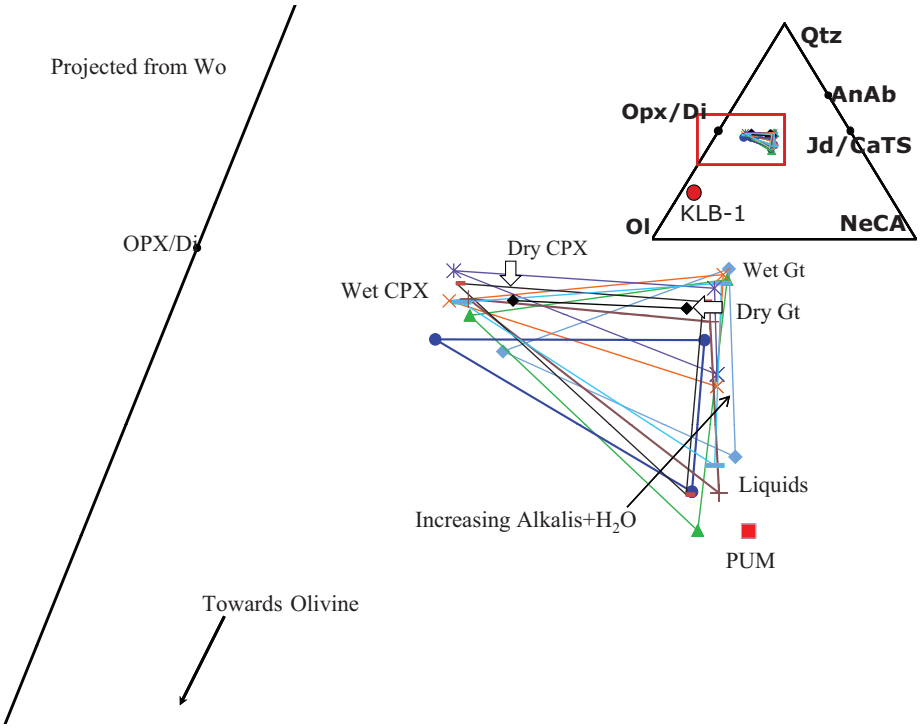

Fig. 10. Solid and liquid compositions from the experiments of this study plotted in the model system olivine–(nepheline–calcium aluminate)–larnite–quartz, as described by Longhi (2002). Abbreviations: Jd/CaTS, jadeite–calcium-tschermakite; AnAb, anorthite–albite; Gt, garnet; OPX, orthopyroxene; Di, diopside; Qtz, quartz; Ol, olivine; NeCA, nepheline–calcium aluminate; Wo, wollastonite; CPX, clinopyroxene. The compositions are projected from wollastonite onto the Ol–Qtz–NeCA plane. Also shown are the compositions of garnet and cpx from our anhydrous recrystallization experiments (black diamonds, labeled with arrows) and the composition of an anhydrous 1% melt of PUM calculated by Longhi (2002) (red square). Each experiment that produced measurements of a liquid, cpx, and garnet composition gives three composition points, shown connected by a triangle. In general, the points move away from the point PUM and away from olivine with increasing total H_2O plus alkali contents, as represented by the arrow. R390 (green triangles) is a notable outlier to this trend. The inset shows the full compositional triangle with the red box delimiting the area illustrated in the larger image.

abundance of garnet without significant impacts on the liquid compositions, second that the spinel-to-garnet transition causes a decrease in liquid Al_2O_3 content, and third that the presence of water has only a small effect on the liquid Al_2O_3. The presence of garnet may impose a limit on liquid Al_2O_3, with only limited changes owing to variable H_2O contents.

Longhi (2002) presented calculations of liquid compositions using his BATCH program that demonstrate the behavior of Al_2O_3. The model recovers the high-melt fraction experimental result of Walter (1998) closely and predicts a notable decrease in liquid Al_2O_3 with decreasing melt fraction. As our volatile-free Al_2O_3 contents are close to those of Walter (1998), this suggests that our experiments may represent slightly elevated degrees of melting. However, liquid Al_2O_3 depends on enough other variables—such as residual garnet mode, cpx composition, presence or absence of opx, and possibly H_2O content—that direct inference of melt fraction from liquid Al_2O_3 is probably not possible. On the basis of other arguments, our multiply saturated melts remain consistent with low-degree melts of hydrous garnet peridotite.

In pHMELTS, liquid Al_2O_3 is much greater than in our experiments, suggesting that the model overestimates the stability of garnet and predicts too little garnet in the melting reaction. pHMELTS also predicts a negative correlation between liquid Al_2O_3 content and water content (Asimow *et al.*, 2004) that is not observed in our experiments.

CaO

CaO shows perhaps the most complex behavior of any oxide in our experiments, and cannot be understood by a simple relationship between a fixed set of solids and a final liquid composition.

At low pressures, a miscibility gap exists between cpx and opx (e.g. Longhi & Bertka, 1996). As pressure increases, the stability field of cpx expands until opx is no longer stable in common peridotites (Longhi & Bertka, 1996), a behavior seen in our subsolidus recrystallization experiments. The peridotite begins as a mixture of olivine, opx, cpx, and spinel, with ~19·5 wt % CaO (Davis *et al.*, 2009) in the initial cpx. After recrystallization at 3 GPa, spinel and opx react out, producing garnet and a cpx with

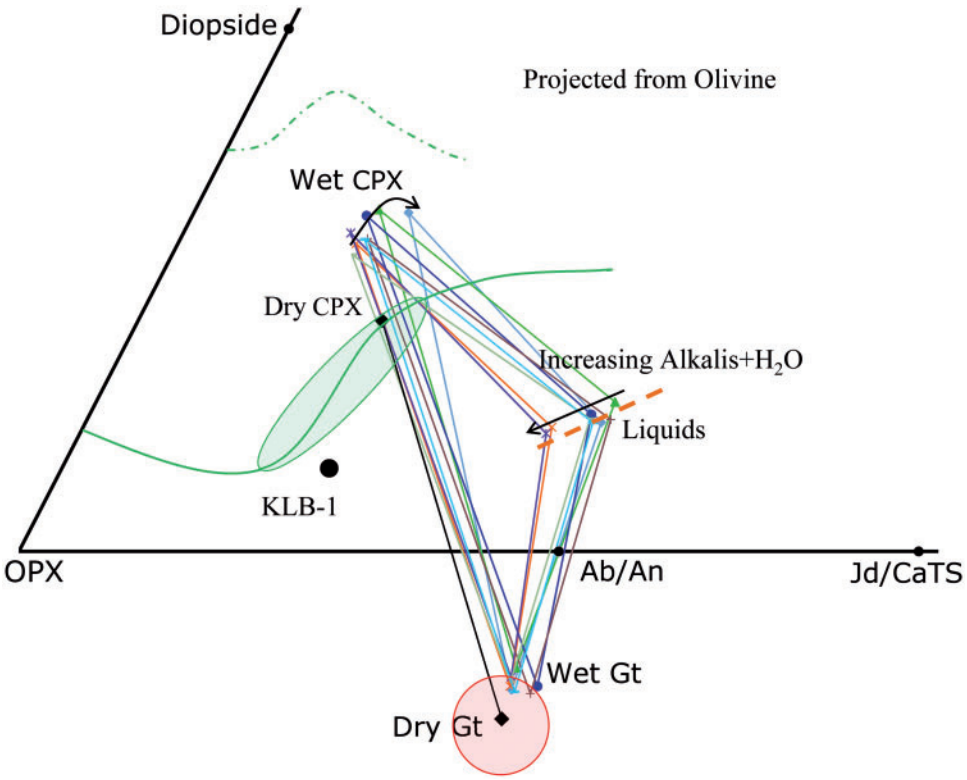

Fig. 11. Solid and liquid compositions plotted in the same normative component space as Fig. 10, but here projected from olivine into the plane OPX–Wo–(Jd–CaTS). Also shown are the composition of our dry cpx and garnet (black diamonds, labeled), the composition of KLB-1 as measured by Davis *et al.* (2009), the fields of cpx (green ellipse) and garnet (red circle) compositions from the 2·8 GPa experiments of Longhi (2002), the edge of the cpx field at 2·8 GPa of Longhi (2002) (continuous green line), the boundary of the cpx field at 0·1 MPa of Longhi (2002) (dashed green line), and the approximate position of the garnet–cpx–olivine cotectic at 2·8 GPa of Longhi (2002) (dashed orange line). Our hydrous experiments produced garnets with slightly more aluminous compositions, but still within the field sampled by Longhi (2002). Our subsolidus cpx composition falls, within error, on the line defining the edge of the 2·8 GPa cpx field. All of the cpx from our wet experiments shift significantly in composition towards diopside and away from albite–anorthite. This shift consists of a change in composition towards lower Al_2O_3 and higher CaO contents in the hydrous experiments. In general, increasing liquid contents of alkalis + H_2O tend to shift the liquid and cpx composition as shown by the arrows; the cpx moves away from OPX whereas the liquid moves towards it. Our liquids project within error on the 2·8 GPa olivine–cpx–garnet cotectic of Longhi (2002).

~12 wt % CaO, consistent with cpx grains measured in anhydrous melting experiments. Our peridotite was recrystallized at a temperature 150°C below the lowest temperature experiment of Walter (1998) and thus shows a slightly higher cpx CaO content, but the pattern is the same. The cpx from our subsolidus experiments also plots very close to the predicted edge of the 2·8 GPa cpx field of Longhi (2002) (Fig. 11). Despite the additional Al_2O_3 in our experiments, the cpx in the subsolidus peridotites is fully consistent with cpx from these other studies.

Gaetani & Grove (1998) noted that there was a slight increase in the CaO content of cpx in their hydrous experiments at 1·6 GPa. However, because the expansion in the dry cpx field occurs mostly at pressures higher than those sampled by their experiments, they observed a minimal effect.

When the cpx in our recrystallized peridotites is exposed to a hydrous silicate melt, it shifts in composition significantly. The cpx in every hydrous experiment contained ~17 wt % CaO. Graphically, this composition plots well inside the anhydrous field boundary for cpx at these pressures; there is a substantial and previously unpredicted contraction of the cpx field solely as a result of the presence of the hydrous melt (Fig. 11).

The increase in cpx CaO content is accompanied by a decrease in its modal abundance and so has two competing effects on the bulk partitioning of CaO. The mineral/melt D_{CaO} increases, but cpx is the phase in which CaO is most compatible, so decreasing its mode lowers the bulk partition coefficient. The balance of these effects favors decreasing liquid CaO content with decreasing cpx CaO content (Walter, 1998). We therefore expect that the increase in cpx CaO in hydrous systems will be accompanied by a small increase in liquid CaO compared with anhydrous experiments, depending on the exact bulk composition.

Comparison with melt compositions from previous experiments suggests that this result is robust. At all conditions, the experimental liquids of Longhi (2002) and calculated liquids from the BATCH program are significantly lower in CaO than our liquids (Fig. 7). Similarly, MELTS calculates much lower CaO contents than seen in our liquids. To confirm that this behavior is controlled by the abundance of cpx, we can also compare the CaO/Al_2O_3 ratio, which may be less sensitive to degree of melting than simply CaO content; indeed, the liquids in Longhi (2002) have significantly lower CaO/Al_2O_3 ratios than those in our experiments, again suggesting higher liquid CaO contents during hydrous melting and confirming that the liquid CaO contents are not elevated as a result of changing melt fraction. In addition, our liquid has a similar CaO content to those of Gaetani & Grove (1998) at lower pressure, but a higher CaO/Al_2O_3 ratio owing to increased Al_2O_3 compatibility in our experiments related to the presence of garnet. This suggests that the melting behavior of our pyroxenes from 3 GPa is similar to that seen by Gaetani & Grove (1998), despite the increased pressure, confirming that these pyroxenes in a water-bearing system are fundamentally different from those in dry systems.

It is more difficult to postulate a mechanism for the behavior of cpx than it is for olivine, as the interaction of olivine with hydrous melts has been much more thoroughly studied. The pyroxene structure is more polymerized than olivine, with oxygen atoms shared between silica tetrahedra. Adding water to a silicate liquid therefore makes the liquid structure less pyroxene-like, which should reduce the stability of cpx. One possible explanation is that as the presence of water decreases the stability of cpx it has a stronger effect on the high-Al_2O_3 cpx, causing the field boundary to retreat towards high-CaO cpx. Alternatively, water could in effect destabilize the opx component in the solid. Longhi (2002) and others have suggested that in anhydrous systems, opx is a product of melting at 3 GPa. If the presence of water instead moved opx back to being a reactant, the melting reaction could proceed by drawing the opx component out of the cpx and into the liquid. This mechanism is illustrated qualitatively by the arrows showing motion of our measured liquid compositions away from olivine and the liquid composition from Longhi (2002) (Fig. 10) and towards opx (Fig. 11) with increasing water content.

Na_2O

The Na_2O content of low-degree silicate melts at high pressure is poorly constrained. Experiments by Robinson *et al.* (1998) suggest that Na_2O is highly incompatible, and the pHMELTS algorithm calculates liquid Na_2O contents that appear unreasonably high (Fig. 7). However, several workers have suggested that D_{Na2O} for cpx increases with increasing pressure. Blundy *et al.* (1995) and Villiger *et al.* (2007) presented calibrations for the increase of D_{Na2O} with pressure, and Longhi (2002) suggested that high cpx D_{Na2O} limits liquid Na_2O contents to ~2·5 wt % above 3 GPa. Although there is some variation owing to changing modal abundances, our liquids contain between 2·47 and 3·24 wt % Na_2O, higher than this limit (Fig. 7). We believe that these Na_2O contents are directly related to the decreasing Al_2O_3 content of the cpx, which decreases the bulk D_{Na2O} as sodium in cpx is charge-balanced by aluminum in a jadeite component. Indeed, the cpx in the anhydrous experiments of Longhi (2002) has higher Na_2O contents than those seen in our experiments, and all three studies predict higher cpx D_{Na2O} than we measured; both Blundy *et al.* (1995) and Villiger *et al.* (2007) predicted cpx D_{Na2O} higher than our values by a factor of two. Although our liquid Na_2O concentrations only mildly exceed the limit proposed by Longhi (2002), our experiments suggest that increasing water contents could correlate with increasing melt Na_2O contents owing to the hydrous contraction of the cpx field. Finally, because the pHMELTS algorithm is not calibrated on experiments that show this high-pressure Na_2O compatibility, it calculates an extremely Na_2O-rich melt, which also produces a corresponding decrease in the calculated melt CaO and Al_2O_3 as a consequence of closure. The lack of calibration for cpx D_{Na2O} in pHMELTS appears to be the single largest source of error in the calculated melt composition.

K_2O

K_2O is the only measured oxide other than the volatiles that is perfectly incompatible at the level of our analytical capability. K_2O varies from 0·25 to 0·5 wt % in our liquids, but even in the most potassic experiment, with high microprobe currents and long counting times, K_2O cannot be statistically distinguished from zero in any solid. Our liquid has more K_2O than the higher degree melts of Gaetani & Grove (1998) but less than the liquids of Longhi (2002) and Walter (1998), reflecting simply differences in the abundance of K_2O in the starting compositions and final solid/liquid ratios (Fig. 7). We therefore have limited constraints on K_2O contents in natural peridotite melts, but there should be corresponding effects of changing K_2O on the other oxides in the liquid similar to those illustrated by the arrows in Figs 10 and 11.

Cr_2O_3

Compared with the measured liquid composition in every other study from 3 GPa considered here, our liquid has significantly less Cr_2O_3 (Fig. 7). Cr_2O_3 is incompatible in olivine, but is compatible in garnet and cpx. Despite the fact that our experiments were conducted outside the stability field of spinel, in which Cr_2O_3 is highly compatible, this cpx and garnet compatibility causes low Cr_2O_3 in our liquids, in particular owing to the effect of garnet. The experiments of Gaetani & Grove (1998) show similarly low

Cr_2O_3 contents but contain spinel in which Cr_2O_3 is strongly compatible. None of the experiments of Walter (1998) or the calculated compositions from the BATCH algorithm of Longhi (2002) yield Cr_2O_3 contents as low as our experiments. The solids measured by Walter (1998) do show Cr_2O_3 contents similar to or greater than those measured in our garnets and cpx, consistent with our Cr_2O_3 contents being controlled by excess garnet. The pHMELTS calculation also gives liquids with much higher Cr_2O_3 contents than we measured, because the algorithm does not include Cr_2O_3-bearing components in any solid other than spinel.

TiO_2

Several models have been proposed to explain TiO_2 partitioning and the TiO_2 content of mantle melts. For example, Gaetani & Grove (1995) and Hill *et al.* (2000) argued that TiO_2 behaves as a trace element in pyroxene with a substitution coupled to Al_2O_3, although Gaetani & Grove (1995) did suggest a possible secondary effect of melt composition on D_{TiO2}. Longhi (2002) instead argued that two competing effects control TiO_2 partitioning; decreasing D_{TiO2} with pressure (and increasing cpx Al_2O_3 content) but increasing D_{TiO2} with increasing liquid alkali content. As our experiments show both cpx Al_2O_3 and liquid Na_2O change in the case of hydrous melting, similar complexity is expected in TiO_2 partitioning.

A starting point for analyzing the partitioning of TiO_2 during hydrous melting is our sub-solidus experiments, with low-CaO cpx. In these experiments, garnet has slightly higher TiO_2 contents than cpx, 0·265 wt % compared with 0·237 wt %, but this difference is barely resolved above analytical error (~0·015%, 1σ). When the solid peridotite reacts with the liquid, the cpx field contracts as described above, and the cpx Al_2O_3 decreases. Longhi's (2002) model predicts that this transition should increase cpx D_{TiO2}; however, our experiments consistently show that cpx D_{TiO2} decreases with decreasing cpx Al_2O_3, consistent with the arguments of Gaetani & Grove (1995) and Hill *et al.* (2000).

Longhi (2002) also proposed that D_{TiO2} increases with increasing liquid alkali content. Our liquids have higher Na_2O than those of Longhi (2002), which should be associated with elevated D_{TiO2} based on this model (Fig. 7). Our measured cpx D_{TiO2} is lower than predicted by the BATCH algorithm; however, the measured values of D_{TiO2} fall within the range of experimental results given by Longhi (2002). This result suggests that melt alkali contents may still affect cpx D_{TiO2}, but the contraction of the pyroxene field dominates.

Because we also observe TiO_2 to be only moderately incompatible in garnet, with similar D_{TiO2} for both garnet and cpx, the additional garnet in our system will affect the liquid TiO_2. Yet, because the mineral–melt partition coefficients for TiO_2 are all measurable, we can use a version of the MISE procedure to project the liquid TiO_2 in melts of normal KLB-1 peridotite. Depending on the solid assemblage, this calculation predicts 1·0–1·5 wt % TiO_2, higher than observed in any of our liquids. Conservatively, we estimate 0·9 wt % TiO_2 for a liquid in equilibrium with KLB-1, but we note that this number is sensitive to small changes in source composition and mineralogy.

While attempting to model fractional crystallization and source trends for the Azores, Asimow *et al.* (2004) noted that the MELTS algorithm shows elevated D_{TiO2} in low-degree liquids. This calculation disagreed with the diamond-trap experiments of Baker *et al.* (1995), which found lower liquid TiO_2 than those observed, even in our garnet-rich experiments. pHMELTS calculates a higher liquid TiO_2 than seen here (Fig. 7), close to our estimated solidus liquid composition, but also includes opx in the solids, which would further decrease the bulk D_{TiO2}. The higher TiO_2 concentrations measured here are therefore consistent with the proposal of Asimow *et al.* (2004) that the experiments of Baker *et al.* (1995) overestimate the compatibility of TiO_2 at low melt fractions, and that the pHMELTS model more accurately predicts low-degree melt TiO_2.

H_2O contents and implications for mantle melting and partitioning

Our experiments contain more water than previous estimates for typical MORB or ocean island basalt (OIB), from 2·7 to 6·0 wt % H_2O (Table 1). The pHMELTS algorithm, for example, predicts near-solidus liquids at similar pressure and temperature with ~2·5 wt % H_2O. If the partition coefficient D_{H2O} is near 0·01, as commonly estimated (e.g. Aubaud *et al.*, 2004; Hirschmann *et al.*, 2009), then the source for a liquid with 5 wt % water would have ~500 ppm H_2O, much higher than the 50–200 ppm estimated for normal MORB source mantle (Michael, 1988; Hirth & Kohlstedt, 1996; Gose *et al.*, 2009).

However, the contraction of the cpx field has important implications for water partitioning. Based in part on the experiments of Gaetani & Grove (1998), several researchers including Aubaud *et al.* (2004), Hauri *et al.* (2006), and O'Leary *et al.* (2010) have proposed that the D_{H2O} between melt and olivine or pyroxene is a strong function of the solid Al_2O_3, owing to charge-coupled substitution of H^+–Al^{3+} for Si^{4+}.

As a consequence of the observed change in cpx composition, the calibrations of Aubaud *et al.* (2004), Hauri *et al.* (2006), and O'Leary *et al.* (2010) predict that D_{H2O} in our experiments should be significantly less than in the experiments of Gaetani & Grove (1998). Although our final liquid did not equilibrate with opx, the opx in a previous iteration had 5–6 wt % Al_2O_3, which in the Hauri or Aubaud calibrations would give $D_{H2O} \sim 0{\cdot}015$ for both pyroxenes (Tables 1 and 2 and Fig. 12). These values are

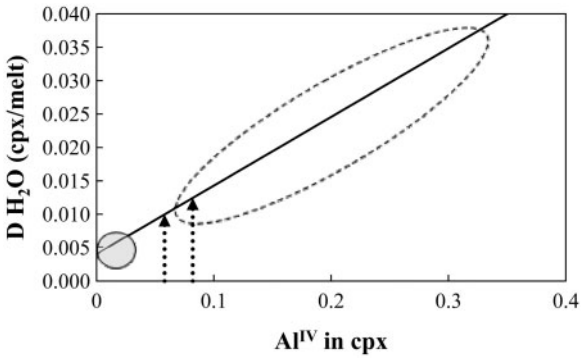

Fig. 12. Projected D_{H2O} as a function of Al^{IV} in cpx based on the correlations of Aubaud *et al.* (2007) and O'Leary *et al.* (2010). Filled gray circle marks the range of low-Al_2O_3 cpx of O'Leary *et al.* (2010). Large dashed oval circle encloses other points in the calibration [see O'Leary *et al.* (2010) for list of data sources]. Dashed vertical lines begin at the measured cpx Al^{IV} from our experiments and project to the correlation line of the above researchers.

significantly lower than those used by Aubaud *et al.* (2004), Hauri *et al.* (2006), Hirschmann *et al.* (2009) or O'Leary *et al.* (2010) to estimate the water storage capacity of the upper mantle and the water content of low-degree melts. Using these partition coefficients, typical peridotite modes, and estimates of olivine and garnet D_{H2O} from those same studies, we calculate a bulk $D_{H2O} \sim 0{\cdot}006$, 50% lower than the value calculated by Aubaud *et al.* (2004) or Hirschmann *et al.* (2009) close to 3 GPa. Based on this partition coefficient, liquid water contents similar to those seen here could still be produced by mantle with typical water contents, possibly down to 100–200 ppm.

Except for the Al-free experiments of O'Leary *et al.* (2010), all cpx synthesized at ~3 GPa contains significantly more Al_2O_3 than our cpx. As a result of increasing pyroxene Al_2O_3 content, Hirschmann *et al.* (2005, 2009) and O'Leary *et al.* (2010) argued that the upper mantle water storage capacity increases with increasing pressure, peaks close to 3 GPa within the garnet lherzolite field, and decreases at pressures greater than 3 GPa as the modal abundance of garnet increases. This water storage capacity peak near 3 GPa would limit hydrous melting to within the spinel lherzolite stability field where the storage capacity is decreased. However, our experiments suggest that the high-Al_2O_3 pyroxenes required for high water storage capacities may not exist when water is present. Consequently, our experiments and calculated D_{H2O} suggest much lower water storage capacities and that any peak would occur at pressures below 3 GPa, within the spinel lherzolite field. With this lower pressure peak, reasonable mantle water contents would drive melting in the garnet stability field, contrary to the suggestion of Hirschmann *et al.* (2009) that peridotites with ~100 ppm water would melt only within the spinel stability field. We caution again that D_{H2O} could not be measured directly in our experiments because of the small run product grain size, but we do note that our experimental techniques could be modified using coarser-grained starting materials to allow for measurement of the actual D_{H2O}. Furthermore, we suggest that experiments within the garnet stability field at temperatures well below the dry solidus are particularly important.

Several workers have estimated bulk D_{H2O} during production of natural basalts by comparing D_{H2O} with REE with similar D values. Michael (1995) suggested that in samples from the Mid-Atlantic Ridge, D_{H2O} was close to D_{Ce}. Danyushevsky *et al.* (2000) measured rocks from the East Pacific Rise and the Southeast Indian Ridge and compared D_{H2O} with D_{Ce}, but also analyzed samples from the Lamont Seamounts and found that D_{H2O} was lower and closer to D_{La}. On the other hand, in back-arc basins, D_{H2O} is close to D_{Nd} and higher than D_{Ce} (Stolper & Newman, 1994). Our data suggest a new mechanism for this variation. Coupled substitution mechanisms with Al_2O_3 in pyroxenes have been proposed for many elements including La and Ce (e.g. Blundy *et al.*, 1998). As a consequence of our reduced pyroxene Al_2O_3, the partitioning of these elements in hydrous, lower-temperature peridotites will differ from partitioning in dry, high-temperature peridotites. Furthermore, becuse hydrogen and REE have different sizes and charges, the D_{REE} will not simply scale with D_{H2O}. The reported variation in relative partition coefficients could therefore be caused by differences in pyroxene Al_2O_3, related to the presence or absence of water.

Dasgupta *et al.* (2007) predicted a strong interaction between water and carbonate during high-pressure carbonate-driven mantle melting. Likewise, we find that water and carbonate behavior are coupled at 3 GPa (e.g. Fig. 6). Specifically, Dasgupta *et al.* (2007) suggested that carbonate melting at depth may extract water and dehydrate peridotites. Carbonated peridotite would then produce very different melts compared with hydrated peridotite, because the removal of dissolved water would prevent the observed cpx field contraction. Furthermore, our data suggest that adding carbonate to a hydrous silicate melt may counteract some of the change in liquid composition by increasing the $(MgO + FeO)/SiO_2$ ratio. The strongest signature of hydrous melting, therefore, would be found in melts sourced from peridotite with high water contents and/or low carbon contents, whereas the presence of moderate amounts of carbon could mask hydrous melt signatures (Dasgupta & Hirschmann, 2007). Further experiments are required on silicate melts with variable ratios of carbonate to water to better constrain this behavior.

Additional implications for mantle melting

Our results suggest that the production of hydrated melts will still occur under mid-ocean ridges at depths of tens of

kilometers below the intersection of an adiabat with the dry solidus. The behavior demonstrated here, including the changing stability of olivine and the unexpected contraction of the cpx composition field, has important implications for the chemistry and depth of melt generation worldwide.

Presence of garnet during melting.

As discussed in the introduction, the presence of a garnet signature in the trace element budget of MORB presents a problem for models based on anhydrous peridotite sources. We show here that hydrous melting is still a possible resolution for this issue.

Kinzler (1997) and previous workers, including Klein & Langmuir (1989), demonstrated that MORB show positive correlations between Na_2O and SiO_2. Furthermore, melts with the highest Na_2O also show the strongest garnet signature (Shen & Forsyth, 1995). This chemistry is qualitatively consistent with our study as the addition of water decreases D_{Na2O} and increases liquid SiO_2. As noted above, as pressure increases Na_2O should become significantly more compatible in anhydrous cpx. In the case of anhydrous melting, therefore, it is particularly difficult to reconcile high liquid Na_2O with the garnet signature, as the liquids produced in the garnet field would have lower Na_2O.

Hydrous melts are thought to be low-degree melts, which consume a large portion of the available water but do not produce large melt volumes. In this way, a hydrous melt can potentially explain the correlation between the increasing garnet signature and decreasing degree of melting (Shen & Forsyth, 1995). Asimow & Langmuir (2003) calculated that for a constant total amount of melt production, increasing the water content of the source led to a decrease in the average degree of melting because the water produced low-degree hydrous melts from large volumes of mantle. If these low-degree melts were generated in the garnet field they would carry the garnet signature; therefore, the wettest and coldest sources would produce low melt fraction liquids that carry the strongest garnet signatures (Fig. 13).

Based on anhydrous experiments, Robinson & Wood (1998) argued that the spinel-to-garnet transition occurs in the pressure range 2·5–3·0 GPa in most peridotites, and that production of significant quantities of melt from the garnet field would require melting at even greater pressures, up to 3·5 GPa, with high potential temperatures that generate implausibly large melt fractions (Fig. 13). However, they also conducted subsolidus experiments and showed that the temperature of the spinel-to-garnet transition is strongly pressure dependent, with a slope of $\sim 400^{\circ}C\,GPa^{-1}$. For the temperature used in our experiments, ~1375°C, extrapolation of their phase boundary predicts a spinel-to-garnet transition at ~2·5 GPa. Furthermore, Gaetani & Grove (1998) produced garnet at pressures as low as 1·6 GPa and temperatures of 1255°C. Therefore, low-temperature, water-driven melting is much more likely to begin within the garnet field and could maintain garnet in the source to much shallower pressures owing to temperature decreases associated with the latent heat of melting.

The partitioning of REE and radioactive isotopes has been a key part of the debate on the garnet signature. Garnet is believed to be the only phase able to retain heavy rare earth elements (HREE) during melting, and therefore a depleted HREE signature in a melt is usually interpreted as indicating residual garnet in the source (e.g. Hirschmann and Stolper, 1996). Compatibility of radioactive elements such as Lu or U can also yield garnet-like signatures by fractionating parent and daughter isotopes (e.g. Salters & Hart, 1989). The attribution of such signatures to garnet of course requires that garnet is the only common phase in the melting zone able to fractionate these elements in the correct sense during melting. Blundy *et al.* (1998) and Wood *et al.* (1999) argued that this was not the case, based on measurements of elevated partition coefficients in aluminous cpx, which could produce a 'garnet signature' without requiring the presence of garnet.

Our cpx compositions bear directly on this issue. In the experiments of Blundy *et al.* (1998), Wood *et al.* (1999), and Hill *et al.* (2000), increased partitioning of HREE and U into highly aluminous cpx was attributed to coupled substitutions involving Na^{+} and Al^{3+}. Similar substitution mechanisms have been proposed for other trace elements in cpx, such as Nb and Ta (Lundstrom *et al.*, 1998) and Hf (Woodhead *et al.*, 2011).Consequently, trace element partitioning in our cpx should be fundamentally different from that in anhydrous systems. Effectively, other cations substituting into cpx would produce trends similar to those for H_2O in Fig. 12, with very low D values in hydrous systems. A specific example of the effect of cpx Al_2O_3 changes can be found in our measured TiO_2 concentrations. As discussed above, the contraction of the cpx stability field leads to decreasing TiO_2 contents in our cpx. Blundy *et al.* (1998) reported high-Al_2O_3 cpx with TiO_2 contents between three and five times higher than those in our cpx, and consequently a cpx D_{TiO2} a factor of 3–5 higher than in our experiments. Although we did not measure trace elements in our experiments, a similar effect on the remaining incompatible elements implies that during hydrous melting cpx cannot create a garnet signature. This effect is similar to that suggested by Green *et al.* (2000), who also noted a lack of variation in cpx D_{HREE} in water-bearing experiments; again suggesting that water-bearing pyroxenes will not generate a garnet signature.

Although this work establishes that H_2O remains a plausible mechanism for the generation of a garnet signature, it does not rule out competing hypotheses. Most

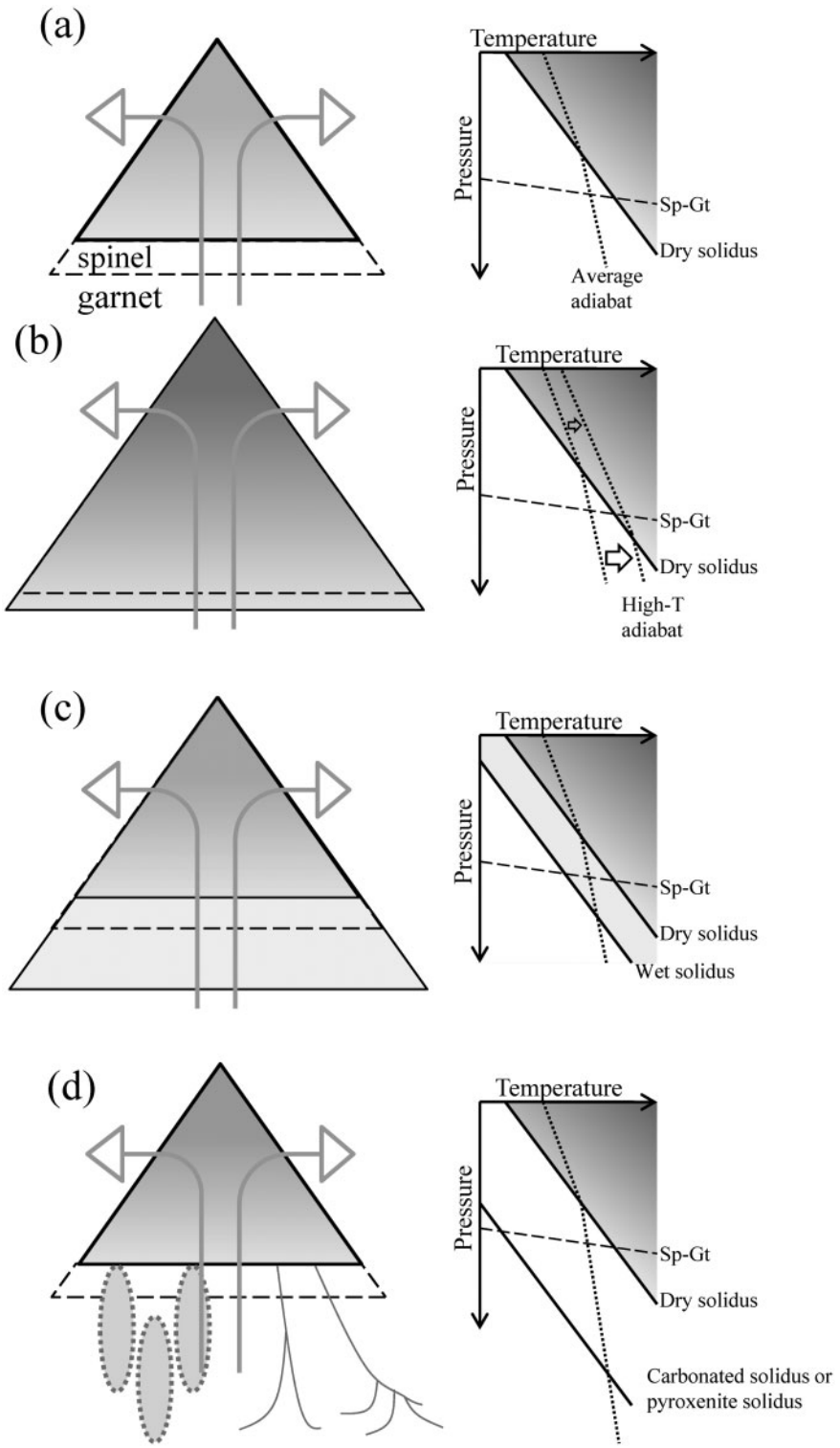

Fig. 13. Schematic triangular and mid-ocean ridge melting zones and production of melt 'garnet signatures'. Triangular regions reflect zones of active melting under hypothetical mid-ocean ridges, shading reflects increasing extent of melting, dashed boundary delineates the spinel-to-garnet transition, arrows show general flow paths of upwelling mantle. Schematic phase diagrams show P–T conditions in each scenario with P and T increasing in the directions of the arrows; solidus curves are shown by continuous lines, the spinel-to-garnet transition by a dashed line, adiabats by dotted lines. (a) Low potential temperature case, either anhydrous or with D_{H2O} values as estimated by Hirschmann *et al.* (2009) or O'Leary *et al.* (2010). (b) High potential temperature case; melting begins in the garnet field. (c) Low potential temperature case with low-degree wet melting tail extending into garnet field; our D_{H2O} values imply substantial solidus depression owing to H_2O. (d) Other possible methods of generating a garnet signature include melting of pyroxenite bodies in the garnet field (ellipses) or carbonate-fluxed melting from great depths (interconnected channels).

notably, small amounts of pyroxenite in the melting source (e.g. Hirschmann & Stolper, 1996; Pertermann & Hirschmann, 2003*b*) and CO_2 or CO_2–H_2O fluxed melting (Dasgupta *et al.*, 2007; Fig. 13) remain plausible, although the observed effect of water-rich melts on cpx may have implications for melting of both pyroxenites and carbonated peridotites. We will consider some of the major element implications here and a specific example of minor element signatures in a companion paper (Balta *et al.*, 2011*a*).

Pyroxenitic sources

If the contraction of the cpx field during hydrous melting is a general phenomenon, it has important implications for pyroxene-rich lithologies. Although we have not explicitly observed cpx-field contraction in a pyroxene-rich lithology, we can qualitatively describe its effects on melting.

A wide variety of natural melt CaO contents have been measured, from very low to melts termed ultra-calcic (Kogiso & Hirschmann, 2001). During peridotite melting, cpx is typically the first phase fully exhausted, with depleted melts produced only after cpx exhaustion (e.g. Asimow *et al.*, 2004). Therefore, more fertile or enriched peridotite sources should also be richer in cpx. Furthermore, cpx-rich lithologies may represent addition of recycled oceanic crust, which could also supply additional water to the source if water were not fully removed during subduction (e.g. Asimow *et al.*, 2004; Hebert *et al.*, 2009). Thus, if enriched sources are also wetter sources, an enriched source could show both cpx Al_2O_3 depletion and increased cpx abundance. In this case, melting of enriched, hydrous sources could produce exceptionally low-CaO liquids. Thus, low-CaO liquids may be most easily produced from hydrous sources, where the source material contains a large quantity of high-CaO cpx. Conversely, the presence of high-CaO cpx in hydrous systems could impose an upper limit on liquid CaO content and render production of ultra-calcic liquids from wet peridotites impossible.

As shown above, the TiO_2 content of liquids is a strong function of the abundance and composition of cpx. The extreme of this behavior is found in pyroxenite melting. Pertermann & Hirschmann (2003*a*) produced very high-TiO_2 (up to 6·7 wt %) liquids coexisting with high-Al_2O_3 cpx. If these melts were hydrous and the D_{TiO2} for cpx decreased further, the resulting liquid would be even richer in TiO_2. High liquid TiO_2 concentrations may therefore be a signature of hydrous melting of pyroxenite sources.

Liquid alkali contents

Previous melting experiments on both peridotite and pyroxenite-rich lithologies result in decreasing liquid Na_2O with increasing pressure owing to increasing cpx D_{Na2O} (Longhi, 2002; Yaxley and Sobolev, 2007). Ideally, this correlation would mean that K_2O/Na_2O in MORB should correlate with melting pressure; however, this ratio does not appear to be as effective as a proxy for pressure (Yaxley and Sobolev, 2007). Our experiments suggest that a major complication to any simple explanation of the alkali ratio is the presence of water. If hydrous melting contracts the stability field of cpx then it will have the opposite effect to increasing pressure on D_{Na2O}; increasing pressure would increase D_{Na2O}, whereas increasing water content would decrease D_{Na2O}. Because hydrous melts are produced at higher pressures than anhydrous melts, these two effects would counteract each other, causing complicated relationships between liquid Na_2O, pressure, and composition. Hydrous melting of pyroxenite lithologies could even lead to elevated Na_2O if the effects of water on cpx are similar to those seen in peridotite, in the opposite direction to that predicted from the simple relationship between K_2O/Na_2O and pressure.

As noted above, K_2O is essentially perfectly incompatible in our experiments, and thus can be treated as a tracer either of source enrichment or of the volume of source sampled. Asimow & Langmuir (2003) showed that hydrous mid-ocean ridge melting will increase the volume of mantle sampled by producing large amounts of low-degree melt. Therefore, the presence of water might increase the K_2O content of erupted liquids at mid-ocean ridges by increasing the volume of peridotite that melts. Alternatively, K_2O and water contents in enriched sources may increase together (Asimow *et al.*, 2004). Increased K_2O in liquids might show correlations with either volatile contents or other indicators of source enrichment, and isolating either of these effects in natural MORB will require better constraints on the relationship between volatiles and source enrichment.

CONCLUSIONS

The presence of water during peridotite melting at 3 GPa produces liquids with an increased SiO_2 content (when normalized to a volatile-free basis) and a decreased $(MgO+FeO)/SiO_2$ ratio compared with anhydrous melts from the same pressure, consistent with the results of hydrous melting experiments at lower pressures. This effect is equivalent to increasing the stability field of olivine relative to the other phases present. The presence of a hydrous melt also has a strong effect on the composition of the equilibrium clinopyroxene. Clinopyroxenes in equilibrium with anhydrous liquids at this pressure have low CaO contents and high Al_2O_3 contents, whereas clinopyroxenes from our hydrous experiments have elevated CaO contents and lower Al_2O_3. The clinopyroxene composition field therefore contracts substantially owing to the presence of water. Trace elements that are hosted in the mantle by clinopyroxene, through coupled substitutions involving Al_2O_3, including water, will therefore have lower partition

coefficients during hydrous melting than during anhydrous melting, and these reduced partition coefficients will strongly affect the water content and the trace element characteristics of any melt produced at this pressure.

ACKNOWLEDGEMENTS

This work benefited from many enlightening discussions with Sally Newman, George Rossman, Mark Hirschmann, Liz Miura, Ma Chi, and Mike Baker. The authors would like to thank Alex Sessions and Magnus Eek for the use of their Elemental Analyzer, Ed Stolper and John Beckett for the use of their 1 atm furnaces, and Claude Herzberg and George Rossman for supplying starting materials. This paper was significantly improved by reviews from Trevor Falloon, Glenn Gaetani, Rajdeep Dasgupta, and Othmar Müntener.

FUNDING

This work was supported by the National Science Foundation Ocean Sciences Marine Geology and Geophysics program, grant numbers OCE-0241716 and OCE-0550216.

SUPPLEMENTARY DATA

Supplementary data for this paper are available at *Journal of Petrology* online.

REFERENCES

Alonso-Perez, R., Müntener, O. & Ulmer, P. (2009). Igneous garnet and amphibole fractionation in the roots of island arcs: experimental constraints on andesitic liquids. *Contributions to Mineralogy and Petrology* **157**, 541–558.

Asimow, P. D. & Langmuir, C. H. (2003). The importance of water to oceanic mantle melting regimes. *Nature* **421**, 815–820.

Asimow, P. D., Hirschmann, M. M., Ghiorso, M. S. & Stolper, E. M. (1999). Calculation of peridotite partial melting from thermodynamic models of minerals and melts. III. Controls on isobaric melt production and the effect of water on melt production. *Journal of Petrology* **40**, 831–851.

Asimow, P. D., Dixon, J. E. & Langmuir, C. H. (2004). A hydrous melting and fractionation model for mid-ocean ridge basalts: application to the Mid-Atlantic Ridge near the Azores. *Geochemistry, Geophysics, Geosystems* **5**, Q01E16.

Aubaud, C., Hauri, E. H. & Hirschmann, M. M. (2004). Hydrogen partition coefficients between nominally anhydrous minerals and basaltic melts. *Geophysical Research Letters* **31**, L20611.

Aubaud, C., Withers, A. C., Hirschmann, M. M., Guan, Y., Leshin, L. A., Mackwell, S. J. & Bell, D. R. (2007). Intercalibration of FTIR and SIMS for hydrogen measurement in glasses and nominally anhydrous minerals. *American Mineralogist* **92**, 811–828.

Baker, M. B. & Stolper, E. M. (1994). Determining the composition of high-pressure mantle melts using diamond aggregates. *Geochimica et Cosmochimica Acta* **58**, 2811–2827.

Baker, M. B., Hirschmann, M. M., Ghiorso, M. S. & Stolper, E. M. (1995). Compositions of near-solidus peridotite melts from experiments and thermodynamic calculations. *Nature* **375**, 308–311.

Balta, J. B., Asimow, P. D. & Mosenfelder, J. L. (2011*a*). Manganese partitioning during hydrous melting of peridotite. *Geochimica et Cosmochimica Acta* (in press), doi:10.1016/j.gca.2011.05.026.

Balta, J. B., Asimow, P. D. & Beckett, J. R. (2011*b*). Thermodynamic properties of alloys of gold-75/palladium-25 with variable amounts of iron and the use of Au–Pd–Fe alloys as containers for experimental petrology. *American Mineralogist* (in press), doi: 10.2138/am.2011.3637.

Bishop, J., Madejová, J., Komadel, P. & Fröschl, H. (2002). The influence of structural Fe, Al and Mg on the infrared OH bands in spectra of dioctahedral smectites. *Clay Minerals* **37**, 607–616.

Blundy, J. D., Falloon, T. J., Wood, B. J. & Dalton, J. A. (1995). Sodium partitioning between clinopyroxene and silicate melts. *Journal of Geophysical Research* **100**, 15501–15515.

Blundy, J. D., Robinson, J. A. C. & Wood, B. J. (1998). Heavy REE are compatible in clinopyroxene on the spinel lherzolite solidus. *Earth and Planetary Science Letters* **160**, 493–504.

Chou, I. (1986). Permeability of precious metals to hydrogen at 2 kb total pressure and elevated temperatures. *American Journal of Science* **286**, 638–658.

Danyushevsky, L. V., Eggins, S. M., Falloon, T. J. & Christie, D. M. (2000). H_2O abundance in depleted to moderately enriched mid-ocean ridge magmas; part I: incompatible behaviour, implications for mantle storage, and origin of regional variations. *Journal of Petrology* **41**, 1329–1364.

Dasgupta, R. & Hirschmann, M. M. (2007). A modified iterative sandwich method for determination of near-solidus partial melt compositions. II. Application to determination of near-solidus melt compositions of carbonated peridotite. *Contributions to Mineralogy and Petrology* **154**, 647–661.

Dasgupta, R., Hirschmann, M. M. & Smith, N. D. (2007). Water follows carbon: CO_2 incites deep silicate melting and dehydration beneath mid-ocean ridges. *Geology* **35**, 135–138.

Davis, F. A., Tangeman, J. A., Tenner, T. J. & Hirschmann, M. M. (2009). The composition of KLB-1 peridotite. *American Mineralogist* **94**, 176–180.

Dixon, J. E., Stolper, E. M. & Holloway, J. R. (1995). An experimental study of water and carbon dioxide solubilities in mid ocean ridge basaltic liquids. 1. Calibration and solubility models. *Journal of Petrology* **36**, 1607–1631.

Dixon, J. E., Clague, D. A., Wallace, P. & Poreda, R. (1997). Volatiles in alkalic basalts form the North Arch Volcanic Field, Hawaii: extensive degassing of deep submarine-erupted alkalic series lavas. *Journal of Petrology* **38**, 911–939.

Falloon, T. J. & Danyushevsky, L. V. (2000). Melting of refractory mantle at 1·5, 2, and 2·5 GPa under anhydrous and H_2O-undersaturated conditions: implications for the petrogenesis of high-Ca boninites and the influence of subduction components on mantle melting. *Journal of Petrology* **41**, 257–283.

Fine, G. & Stolper, E. M. (1986). Dissolved carbon dioxide in basaltic glasses: concentrations and speciation. *Earth and Planetary Science Letters* **76**, 263–278.

Frost, D. J. & McCammon, C. A. (2008). The redox state of Earth's mantle. *Annual Review of Earth and Planetary Sciences* **36**, 389–420.

Gaetani, G. A. & Grove, T. L. (1995). Partitioning of rare earth elements between clinopyroxene and silicate melt: crystal-chemical controls. *Geochimica et Cosmochimica Acta* **59**, 1951–1962.

Gaetani, G. A. & Grove, T. L. (1998). The influence of water on melting of mantle peridotite. *Contributions to Mineralogy and Petrology* **131**, 323–346.

Ghiorso, M. S., Carmichael, I. S. E., Rivers, M. L. & Sack, R. O. (1983). The Gibbs free energy of mixing of natural silicate liquids; an expanded regular solution method for the calculation of magmatic intensive variables. *Contributions to Mineralogy and Petrology* **84**, 107–145.

Ghiorso, M. S., Hirschmann, M. M., Reiners, P. W. & Kress, V. C., III (2002). The pMELTS: A revision of MELTS for improved calculation of phase relations and major element partitioning related to partial melting of the mantle to 3 GPa. *Geochemistry, Geophysics, Geosystems* **3**, 1030.

Gose, J., Schmädicke, E. & Beran, A. (2009). Water in enstatite from Mid-Atlantic Ridge peridotite: evidence for the water content of suboceanic mantle? *Geology* **37**, 543–546.

Green, T. H., Blundy, J. D., Adam, J. & Yaxley, G. M. (2000). SIMS determination of trace element partition coefficients between garnet, clinopyroxene and hydrous basaltic liquids at 2–7·5 GPa and 1080–1200°C. *Lithos* **53**, 165–187.

Hauri, E. H., Gaetani, G. A. & Green, T. H. (2006). Partitioning of water during melting of the Earth's upper mantle at H_2O-undersaturated conditions. *Earth and Planetary Science Letters* **248**, 715–734.

Hebert, L. B., Antoshechkina, P., Asimow, P. & Gurnis, M. (2009). Emergence of a low-viscosity channel in subduction zones through the coupling of mantle flow and thermodynamics. *Earth and Planetary Science Letters* **278**, 243–256.

Herzberg, C. (2000). New experimental observations on the anhydrous solidus for peridotite KLB-1. *Geochemistry, Geophysics, Geosystems* **1**, 1051.

Herzberg, C. (2006). Petrology and thermal structure of the Hawaiian plume from Mauna Kea volcano. *Nature* **444**, 605–609.

Hill, E., Wood, B. J. & Blundy, J. D. (2000). The effect of Ca-Tschermaks component on trace element partitioning between clinopyroxene and silicate melt. *Lithos* **53**, 203–215.

Hirose, K. & Kushiro, I. (1993). Partial melting of dry peridotites at high pressures—determination of compositions of melts segregated from peridotite assemblage using aggregates of diamond. *Earth and Planetary Science Letters* **114**, 477–489.

Hirschmann, M. M. & Dasgupta, R. (2007). A modified iterative sandwich method for determination of near-solidus partial melt compositions. I. Theoretical considerations. *Contributions to Mineralogy and Petrology* **154**, 635–645.

Hirschmann, M. M. & Stolper, E. M. (1996). A possible role for garnet pyroxenite in the origin of the 'garnet signature' in MORB. *Contributions to Mineralogy and Petrology* **124**, 185–208.

Hirschmann, M. M., Baker, M. B. & Stolper, E. M. (1998). The effect of alkalis on the silica content of mantle-derived melts. *Geochimica et Cosmochimica Acta* **62**, 883–902.

Hirschmann, M. M., Aubaud, C. & Withers, A. C. (2005). Storage capacity of H_2O in nominally anhydrous minerals in the upper mantle. *Earth and Planetary Science Letters* **236**, 167–181.

Hirschmann, M. M., Tenner, T., Aubaud, C. & Withers, A. C. (2009). Dehydration melting of nominally anhydrous mantle: the primacy of partitioning. *Physics of the Earth and Planetary Interiors* **176**, 54–68.

Hirth, G. & Kohlstedt, D. L. (1996). Water in the oceanic upper mantle: implications for rheology, melt extraction and the evolution of the lithosphere. *Earth and Planetary Science Letters* **144**, 93–108.

Holloway, J. & Kawamoto, T. (1997). Melting temperature and partial melt chemistry of H_2O-saturated mantle peridotite to 11 gigapascals. *Science* **276**, 240–243.

Humayun, M., Qin, L. & Norman, M. D. (2004). Geochemical evidence for excess iron in the mantle beneath Hawaii. *Science* **306**, 91–94.

Iwamori, H., McKenzie, D. & Takahashi, E. (1995). Melt generation by isentropic mantle upwelling. *Earth and Planetary Science Letters* **134**, 253–266.

Johnson, K. T. M. & Kushiro, I. (1992). Segregation of high-pressure partial melts from peridotite using aggregates of diamond—a new experimental approach. *Geophysical Research Letters* **19**, 1703–1706.

Kägi, R., Muntener, O., Ulmer, P. & Ottolini, L. (2005). Piston-cylinder experiments on H_2O undersaturated Fe-bearing systems: an experimental setup approaching $f(O_2)$ conditions of natural calc-alkaline magmas. *American Mineralogist* **90**, 708–717.

Kelemen, P. B., Dick, H. J. B. & Quick, J. E. (1992). Formation of harzburgite by pervasive melt/rock reaction in the upper mantle. *Nature* **358**, 635–641.

Kelly, S. D., Parker, I. G., Sharman, M. & Dennis, M. J. (1998). On-line quantitative determination of $^2H/^1H$ isotope ratios in organic and water samples using an elemental analyser coupled to an isotope ratio mass spectrometer. *Journal of Mass Spectrometry* **33**, 735–738.

Kessel, R., Beckett, J. R. & Stolper, E. M. (2001). Thermodynamic properties of the Pt–Fe system. *American Mineralogist* **86**, 1003–1014.

Kinzler, R. J. (1997). Melting of mantle peridotite at pressures approaching the spinel to garnet transition: application to mid-ocean ridge basalt petrogenesis. *Journal of Geophysical Research* **102**, 853–874.

Kinzler, R. J. & Grove, T. L. (1992). Primary magmas of mid-ocean ridge basalts 2. Applications. *Journal of Geophysical Research* **97**, 6907–6926.

Klein, E. M. & Langmuir, C. H. (1989). Local versus global variations in ocean ridge basalt composition: a reply. *Journal of Geophysical Research* **94**, 4241–4252.

Kogiso, T. & Hirschmann, M. M. (2001). Experimental study of clinopyroxenite partial melting and the origin of ultra-calcic melt inclusions. *Contributions to Mineralogy and Petrology* **142**, 347–360.

Koziol, A. M. & Newton, R. C. (1988). Redetermination of the anorthite breakdown reaction and improvement of the plagioclase–garnet–Al_2SiO_5–quartz geobarometer. *American Mineralogist* **73**, 216–223.

Kushiro, I. (1968). Compositions of magmas formed by partial melting of the Earth's upper mantle. *Journal of Geophysical Research* **73**, 619–634.

Kushiro, I. (1969). System forsterite–diopside–silica with and without water at high pressures. *American Journal of Science* **267A**, 269–294.

Kushiro, I. (1972). Effect of water on the composition of magmas formed at high pressures. *Journal of Petrology* **13**, 311–334.

Kushiro, I. & Hirose, K. (1992). Experimental determination of composition of melt formed by equilibrium partial melting of peridotite at high pressures using aggregates of diamond grains. *Proceedings of the Japan Academy Series B, Physical and Biological Sciences* **68**, 63–68.

Laporte, D., Toplis, M., Seyler, M. & Devidal, J.-L. (2004). A new experimental technique for extracting liquids from peridotite at very low degrees of melting: application to partial melting of depleted peridotite. *Contributions to Mineralogy and Petrology* **146**, 463–484.

Liu, X., O'Neill, H. S. C. & Berry, A. J. (2006). The effects of small amounts of H_2O, CO_2 and Na_2O on the partial melting of spinel lherzolite in the system $CaO–MgO–Al_2O_3–SiO_2 \pm H_2O \pm CO_2 \pm Na_2O$ at 1·1 GPa. *Journal of Petrology* **47**, 409–434.

Longhi, J. (2002). Some phase equilibrium systematics of lherzolite melting: I. *Geochemistry, Geophysics, Geosystems* **3**, 1020.

Longhi, J. & Bertka, C. M. (1996). Graphical analysis of pigeonite–augite liquidus equilibria. *American Mineralogist* **81**, 685–695.

Lundstrom, C. C., Shaw, H. F., Ryerson, F. J., Williams, Q. & Gill, J. (1998). Crystal chemical control of clinopyroxene–melt

partitioning in the Di–Ab–An system: implications for elemental fractionations in the depleted mantle. *Geochimica et Cosmochimica Acta* **62**, 2849–2862.

Michael, P. J. (1988). The concentration, behavior and storage of H_2O in the suboceanic upper mantle: implications for mantle metasomatism. *Geochimica et Cosmochimica Acta* **52**, 555–566.

Michael, P. J. (1995). Regionally distinctive sources of depleted MORB—evidence from trace-elements and H_2O. *Earth and Planetary Science Letters* **131**, 301–320.

Morizet, Y., Kohn, S. C. & Brooker, R. A. (2001). Annealing experiments on CO_2-bearing jadeite glass: an insight into the true temperature dependence of CO_2 speciation in silicate melts. *Mineralogical Magazine* **65**, 701–707.

Morizet, Y., Brooker, R. A. & Kohn, S. C. (2002). CO_2 in haplophonolite melt: solubility, speciation and carbonate complexation. *Geochimica et Cosmochimica Acta* **66**, 1809–1820.

Mysen, B. O., Virgo, D., Harrison, W. J. & Scarfe, C. M. (1980). Solubility mechanism of H_2O in silicate melts at high pressures and temperatures: a Raman spectroscopic study. *American Mineralogist* **65**, 900–914.

Ohlhorst, S., Behrens, H. & Holtz, F. (2001). Compositional dependence of molar absorptivities of near-infrared OH^- and H_2O bands in rhyolitic to basaltic glasses. *Chemical Geology* **174**, 5–20.

O'Leary, J. A., Gaetani, G. A. & Hauri, E. H. (2010). The effect of tetrahedral Al^{3+} on the partitioning of water between clinopyroxene and silicate melt. *Earth and Planetary Science Letters* **297**, 111–120.

Parman, S. W. & Grove, T. L. (2004). Harzburgite melting with and without H_2O: experimental data and predictive modeling. *Journal of Geophysical Research* **109**, B02201.

Pertermann, M. & Hirschmann, M. M. (2003*a*). Anhydrous partial melting experiments on MORB-like eclogite: phase relations, phase compositions and mineral–melt partitioning of major elements at 2–3 GPa. *Journal of Petrology* **44**, 2173–2201.

Pertermann, M. & Hirschmann, M. M. (2003*b*). Partial melting experiments on a MORB-like pyroxenite between 2 and 3 GPa: constraints on the presence of pyroxenite in basalt source regions from solidus location and melting rate. *Journal of Geophysical Research* **108**, 2125.

Putirka, K., Johnson, M., Kinzler, R., Longhi, J. & Walker, D. (1996). Thermobarometry of mafic igneous rocks based on clinopyroxene–liquid equilibria, 0–30 kbar. *Contributions to Mineralogy and Petrology* **123**, 92–108.

Robinson, J. A. C. & Wood, B. J. (1998). The depth of the spinel to garnet transition at the peridotite solidus. *Earth and Planetary Science Letters* **164**, 277–284.

Robinson, J. A. C., Wood, B. J. & Blundy, J. D. (1998). The beginning of melting of fertile and depleted peridotite at 1·5 GPa. *Earth and Planetary Science Letters* **155**, 97–111.

Salters, V. J. M. & Hart, S. R. (1989). The hafnium paradox and the role of garnet in the source of mid-ocean-ridge basalts. *Nature* **342**, 420–422.

Salters, V. J. M. & Longhi, J. (1999). Trace element partitioning during the initial stages of melting beneath mid-ocean ridges. *Earth and Planetary Science Letters* **166**, 15–30.

Schwab, B. E. & Johnston, A. D. (2001). Melting systematics of modally variable, compositionally intermediate peridotites and the effects of mineral fertility. *Journal of Petrology* **42**, 1789–1811.

Sessions, A. L. (2006). Isotope-ratio detection for gas chromatography. *Journal of Separation Science* **29**, 1946–1961.

Shen, Y. & Forsyth, D. W. (1995). Geochemical constraints on initial and final depths of melting beneath mid-ocean ridges. *Journal of Geophysical Research* **100**, 2211–2237.

Sisson, T. W., Ratajeski, K., Hankins, W. B. & Glazner, A. F. (2005). Voluminous granitic magmas from common basaltic sources. *Contributions to Mineralogy and Petrology* **148**, 635–661.

Smith, P. M. & Asimow, P. D. (2005). Adiabat_1ph: A new front end to the MELTS, pMELTS, and pHMELTS models. *Geochemistry, Geophysics, Geosystems* **6**, Q02004.

Stolper, E. (1980). A phase diagram for mid-ocean ridge basalts: preliminary results and implications for petrogenesis. *Contributions to Mineralogy and Petrology* **74**, 13–27.

Stolper, E. & Newman, S. (1994). The role of water in the petrogenesis of Mariana Trough magmas. *Earth and Planetary Science Letters* **121**, 293–325.

Takahashi, E. & Kushiro, I. (1983). Melting of a dry peridotite at high pressures and basalt magma genesis. *American Mineralogist* **69**, 859–879.

Toplis, M. J. (2005). The thermodynamics of iron and magnesium partitioning between olivine and liquid: criteria for assessing and predicting equilibrium in natural and experimental systems. *Contributions to Mineralogy and Petrology* **149**, 22–39.

Tsuchiyama, A., Nagahara, H. & Kushiro, I. (1981). Volatilization of sodium from silicate melt spheres and its application to the formation of chondrules. *Geochimica et Cosmochimica Acta* **45**, 1357–1367.

Van den Bleeken, G., Müntener, O. & Ulmer, P. (2011). Melt variability in percolated peridotite: an experimental study applied to reactive migration of tholeiitic basalt in the upper mantle. *Contributions to Mineralogy and Petrology* **161**, 1–25.

Villiger, S., Ulmer, P. & Müntener, O. (2007). Equilibrium and fractional crystallization experiments at 0·7 GPa; the effect of pressure on phase relations and liquid compositions of tholeiitic magmas. *Journal of Petrology* **48**, 159–184.

Wallace, M. E. & Green, D. H. (1988). An experimental determination of primary carbonatite magma composition. *Nature* **335**, 343–346.

Walter, M. J. (1998). Melting of garnet peridotite and the origin of komatiite and depleted lithosphere. *Journal of Petrology* **39**, 29–60.

Wasylenki, L., Baker, M., Kent, A. & Stolper, E. (2003). Near-solidus melting of the shallow upper mantle: partial melting experiments on depleted peridotite. *Journal of Petrology* **44**, 1163–1191.

White, R. S., McKenzie, D. & O'Nions, R. K. (1992). Oceanic crustal thickness from seismic measurements and rare earth element inversions. *Journal of Geophysical Research* **97**, 19683–19715.

Withers, A. C., Hirschmann, M. M. & Behrens, H. (2009). Hydrous glass standards for microanalysis of hydrogen. *EOS Transactions, American Geophysical Union* V31E-2016 (abstract).

Wood, B. J. & Turner, S. P. (2009). Origin of primitive high-Mg andesite: Constraints from natural examples and experiments. *Earth and Planetary Science Letters* **283**, 59–66.

Wood, B. J., Blundy, J. D. & Robinson, J. A. C. (1999). The role of clinopyroxene in generating U-series disequilibrium during mantle melting. *Geochimica et Cosmochimica Acta* **63**, 1613–1620.

Woodhead, J., Hergt, J., Greig, A. & Edwards, L. (2011). Subduction zone Hf-anomalies: mantle messenger, melting artefact or crustal process? *Earth and Planetary Science Letters* **304**, 231–239.

Yaxley, G. & Sobolev, A. (2007). High-pressure partial melting of gabbro and its role in the Hawaiian magma source. *Contributions to Mineralogy and Petrology* **154**, 371–383.